Synthesis and Reactivity of [*closo*-1-CB$_9$H$_9$-1-N$_2$]: Functional Group Interconversion at the Carbon Vertex of the {*closo*-1-CB$_9$} Cluster

Bryan Ringstrand, Piotr Kaszynski,* and Andreas Franken

Organic Materials Research Group Department of Chemistry, Vanderbilt University, Nashville, Tennessee 37235

The dinitrogen derivative [*closo*-1-CB$_9$H$_9$-1-N$_2$] (**1**) was prepared from amine [*closo*-1-CB$_9$H$_9$-1-NH$_3$] (**2**) and reacted with three types of nucleophiles: activated arenes (phenolate and aniline), divalent sulfur compounds (Me$_2$S and Me$_2$NCHS), and pyridine, giving products of substitution at C$_{cage}$. The reaction of **1** with pyridine gave all four isomers **11a**−**11d**, indicating the Gomberg−Bachmann mechanism, which involves radical anion [*closo*-1-CB$_9$H$_9$]$^{-•}$ (**26**). The radical and also closed-shell electrophilic aromatic substitution mechanisms were probed with the aid of DFT and MP2 computational methods and compared to those of phenylation of pyridine. Overall, experimental results supported by computational analysis suggest two mechanisms for the substitution of the N$_2$ group in **1**: (*i*) thermal heterolytic cleavage of the C$_{cage}$−N bond and the formation of electrophilic carbonium ylide [*closo*-1-CB$_9$H$_9$] (**19**) and (*ii*) electron-transfer-induced homolytic cleavage of the C$_{cage}$−N bond and the formation of **26**. Decomposition of **1** in MeCN is believed to proceed by the nonradical mechanism involving formation of the ylide **19** as the rate-determining step with experimental activation parameters $\triangle H^{\ddagger} = 38.4 \pm 0.8$ kcal mol^{-1} and $\triangle S^{\ddagger} = 44.5 \pm 2.5$ cal mol^{-1} K^{-1}. The electron-transfer-induced formation of **26** is consistent with the relatively high reduction potential of **1** ($E_{pc} = -0.54$ V), which is more cathodic than that of PhN$_2$$^+$ by 0.38 V. Transformations of the phenol **8a** and the Me$_2$NCHS adduct **10** were demonstrated by *O*-methylation of the former and hydrolysis of **10** followed by *S*-alkylative cyclization. Direct products and their derivatives were investigated by UV−vis spectroscopy and analyzed with the ZINDO computational method.

Introduction

Dinitrogen derivatives of the [*closo*-B$_{10}$H$_{10}$]$^{2-}$ cluster are isolable stable[1−6] and important intermediates in the preparation of a variety of nitrogen,[1−4,6−8] sulfur,[4,6,8,9] oxygen,[4,10] and even carbon[4] derivatives. Our calculations showed that the moderate stability and hence synthetic usefulness of these intermediates originate from the electronic interaction between the cluster and the N$_2$ group, which appears to be general for the apical position of 10-vertex *closo*-boranes.[11] Indeed, scant indirect evidence suggests that [*closo*-1-CB$_9$H$_9$-1-N$_2$] (**1**), formed by diazotization of amine [*closo*-1-CB$_9$H$_9$-1-NH$_3$] (**2**), is also reasonably stable and was implied as an intermediate in a reaction with Me$_2$S.[12] Therefore, in analogy to the dinitrogen derivatives of [*closo*-B$_{10}$H$_{10}$]$^{2-}$, compound **1** and its derivatives have the potential of becoming synthetically valuable intermediates in the introduction of substituents at the C$_{cage}$ position of the {*closo*-1-CB$_9$} cage.

Our interest[7,8,13−15] in highly polar and ionic molecular materials, including liquid crystals, focused our attention on dinitrogen derivatives **I**, 10-substituted derivatives of **1**, as potential intermediates in the synthesis of zwitterionic and anionic azo compounds of the general structures **II** and **III**, respectively (Figure 1). In this context, we recently developed[15,16] synthetic access to isomerically pure [*closo*-1-CB$_9$H$_8$-1-NH$_2$-10-I]$^-$ as the

*To whom correspondence should be addressed. Phone: (615) 322-3458. Fax: (615) 343-1234. E-mail: piotr.kaszynski@vanderbilt.edu.

(1) Hertler, W. R.; Knoth, W. H.; Muetterties, E. L. *J. Am. Chem. Soc.* **1964**, *86*, 5434–5439.
(2) Hertler, W. R.; Knoth, W. H.; Muetterties, E. L. *Inorg. Chem.* **1965**, *4*, 288–293.
(3) Knoth, W. H.; Hertler, W. R.; Muetterties, E. L. *Inorg. Chem.* **1965**, *4*, 280–287.
(4) Knoth, W. H. *J. Am. Chem. Soc.* **1966**, *88*, 935–939.
(5) Leyden, R. N.; Hawthorne, M. F. *Inorg. Chem.* **1975**, *14*, 2444–2446.
(6) Balinski, A.; Januszko, A.; Harvey, J. E.; Brady, E.; Kaszynski, P.; Young, V. G., Jr. Manuscript in preparation.
(7) Kaszynski, P.; Huang, J.; Jenkins, G. S.; Bairamov, K. A.; Lipiak, D. *Mol. Cryst. Liq. Cryst.* **1995**, *260*, 315–331.
(8) Kaszynski, P.; Douglass, A. G. *J. Organomet. Chem.* **1999**, *581*, 28–38.
(9) Komura, M.; Nakai, H.; Shiro, M. *J. Chem. Soc., Dalton Trans.* **1987**, 1953–1956.
(10) Bragin, V. I.; Sivaev, I. B.; Bregadze, V. I.; Votinova, N. A. *J. Organomet. Chem.* **2005**, *690*, 2847–2849.
(11) Kaszynski, P.; Pakhomov, S.; Young, V. G., Jr. *Collect. Czech. Chem. Commun.* **2002**, *67*, 1061–1083.

(12) Jelinek, T.; Stibr, B.; Plesek, J.; Thornton-Pett, M.; Kennedy, J. D. *J. Chem. Soc., Dalton Trans.* **1997**, 4231–4236.
(13) Kaszynski, P.; Lipiak, D. In *Materials for Optical Limiting*; Crane, R., Lewis, K., Stryland, E. V., Khoshnevisan, M., Eds.; MRS: Boston, 1995; Vol. *374*, pp 341–347.
(14) Fendrich, W.; Harvey, J. E.; Kaszynski, P. *Inorg. Chem.* **1999**, *38*, 408–410.
(15) Ringstrand, B.; Kaszynski, P. *J. Mater. Chem.* **2009**, *19*, 4805–4812.
(16) Ringstrand, B.; Balinski, A.; Franken, A.; Kaszynski, P. *Inorg. Chem.* **2005**, *44*, 9561–9566.
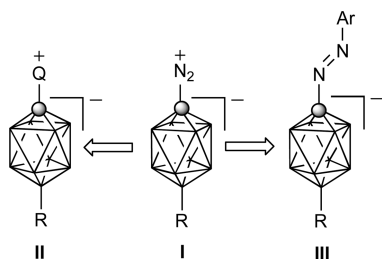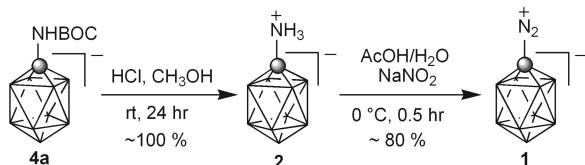
Figure 1. General structures for the polar and ionic derivatives **II** and **III** and their precursor **I**. Q^+ represents an onium fragment such as quinuclidinium, pyridinium, or sulfonium.

Scheme 1

Scheme 2

key starting material for the preparation of **II** and **III**. In this precursor, the amino group is expected to serve as a synthetic handle for the introduction of a sulfonium fragment, a pyridin-1-yl group, and an azo group through the dinitrogen derivative **I**. Therefore, we desired to gain an understanding of the properties and reactivity of **1** as a model for **I** and a step toward the development of synthetic access to **II** and **III**.

Here, we report a reliable method for the preparation of amine **2**, which upon diazotization gives [*closo*-1-CB$_9$H$_9$-1-N$_2$] (**1**). Then, we describe the thermal stability and reactivity of dinitrogen derivative **1** with several nucleophilic reagents. In particular, we explored reactions that lead to derivatives with the protected mercapto functionality, diazocoupling to aromatic compounds, and reactions with pyridine. The mechanism of the reaction of **1** with pyridine was investigated experimentally and analyzed with the aid of DFT and MP2 computational methods. The dinitrogen derivative **1** and several products derived from it were investigated with UV−vis spectroscopic methods, and the experimental results were compared to the ZINDO computational data. Finally, the transmission of the C$_{cage}$ substituent electronic effects through the {*closo*-1-CB$_9$} cage was briefly investigated and compared to that of {*closo*-1-CB$_{11}$} and the benzene ring.

Results

Synthesis of [*closo*-1-CB$_9$H$_9$-1-N$_2$] (1). The preparation of [*closo*-1-CB$_9$H$_9$-1-N$_2$] (**1**) was accomplished by diazotization of [*closo*-1-CB$_9$H$_9$-1-NH$_3$] (**2**) in a 50% aqueous AcOH with 1.1 equiv of NaNO$_2$ (Scheme 1). The dinitrogen derivative **1** was formed as a white precipitate and conveniently isolated by filtration in yields > 80%. Diazotization of contaminated amine **2**, for example, with carboxylic acid **3**, also was satisfactory, albeit with lower yields of **1**, since the ionic impurity tends to stay in solution. The ratio and amounts of AcOH and H$_2$O were optimized to maximize the material recovery.

The dinitrogen derivative **1** is a white microcrystalline substance easily soluble in common organic solvents, except for alkanes. It is stable in the solid state at 0 °C for at least 18 months without traces of decomposition. When heated, solid **1** rapidly decomposes at 87 °C. Its
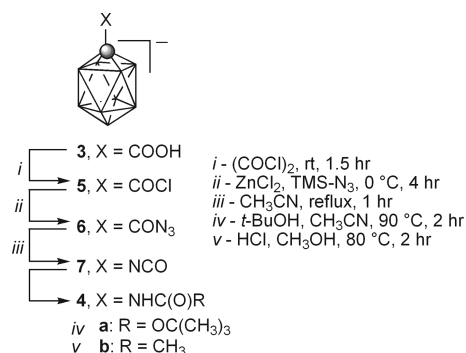
solutions in MeCN are stable for 24 h at ambient temperature in the dark with little (about 10%) decomposition (vide infra). In contrast, dinitrogen **1** completely decomposes in CH$_2$Cl$_2$ and benzene solutions into a mostly intractable mixture of presumably polymeric and degradation products after 24 h in the dark at ambient temperatures. NMR spectra of **1** display a significant solvent dependence. Thus, the signals of ^{11}B(10) and ^{1}H(10) nuclei are shifted by about 6 and 1.2 ppm, respectively, downfield in benzene-d_6 relative to those measured in CD$_3$CN solutions.

Although amine **2** has been reported in the literature,[12] its previous preparation was complicated by the formation of the closely related [*closo*-1-CB$_{11}$H$_{11}$-1-NH$_3$] as a byproduct. Also, this method does not allow for introduction of a substituent at the B(10) position. Therefore, we decided to develop reliable access to **2** starting from the readily accessible carboxylic acid **3**.[16] Our initial attempts at direct conversion of carboxylic acid **3** to amine **2** using several methods such as the classical Schmidt[17] and Curtius reactions,[18] azidotrimethylsilane,[19] azidotrimethylsilane and NaN$_3$,[20] diphenylphosphoryl azide,[21] and hydroxylamine sulfonic acid[22] were unsatisfactory and plagued by poor yields, irreproducibility, low reactivity with acid **3[NEt$_4$]**, and numerous unidentified side products, as evident from ^{11}B NMR. Eventually, we focused on the Curtius reaction and carbamate **4** as the isolable intermediate, which could be purified and serve as a convenient storage for amine **2**. Conditions for each synthetic step were optimized, and the reactions were followed by monitoring the chemical shifts of the B(10) nucleus in ^{11}B NMR spectra and the IR vibrations of the carbonyl group (see the Supporting Information). Thus, the required carbamate **4a[NEt$_4$]** was prepared in four steps and about 50% overall yield based on carboxylic acid **3[NEt$_4$]** using a modified Curtius rearrangement (Scheme 2).

The first step of the preparation of carbamate **4a[NEt$_4$]** was the typically quantitative transformation of carboxylic

(17) Banthorpe, D. V. In *The Chemistry of the Azido Group*; Patai, Ed.; Wiley: New York, 1971; p 405.
(18) Banthorpe, D. V. In *The Chemistry of the Azido Group*; Patai, Ed.; Wiley: New York, 1971; p 397.
(19) Krow, G.; Damodaran, K. M.; Michener, E.; Miller, S. I.; Dalton, D. R. *Synth. Commun.* **1976**, *6*, 261–267.
(20) Warren, J. D.; Press, J. B. *Synth. Commun.* **1980**, *10*, 107–110.
(21) Shioiri, T.; Ninomiya, K.; Yamada, S. *J. Am. Chem. Soc.* **1972**, *94*, 6203–6205.
(22) Wallace, R. G.; Barker, J. M.; Wood, M. L. *Synthesis* **1990**, *12*, 1143–1144.

acid **3[NEt₄]** to carbonyl chloride **5[NEt₄]** using $(COCl)_2$. The crude chloride **5[NEt₄]** was then converted to acyl azide **6[NEt₄]** using Me_3SiN_3 in the presence of $ZnCl_2$ according to a general literature procedure.[23] ^{11}B NMR spectra typically showed 85% conversion to the azide **6[NEt₄]**, with the remaining chloride **5[NEt₄]** being hydrolyzed back to acid **3[NEt₄]**. A minor peak at 25.1 ppm in ^{11}B NMR spectra of the crude reaction mixture was also present, which was later attributed to isocyanate **7[NEt₄]**. The premature rearrangement of azide **6[NEt₄]** to **7[NEt₄]** was most likely promoted by the Lewis acid catalyst rather than thermal induction.[24]

Attempts at improving this process through manipulation with reaction times, catalyst loading, and thorough drying of the catalyst were unsuccessful. The IR spectrum of azide **6[NEt₄]** revealed vibrations characteristic for the azido and carbonyl groups and is similar to that reported for benzoyl azide.[25]

Crude azide **6[NEt₄]** was rearranged to isocyanate **7[NEt₄]** by refluxing in anhydrous CH_3CN. The completeness of the transformation was evident from ^{11}B NMR spectra in which the B(10) chemical shift of the former at 36.4 ppm was replaced with a peak at 25.1 ppm in the isocyanate. The product also showed an intense peak at 2262 cm^{-1} in the IR spectrum, which is consistent with the ν_{NCO} vibration reported for phenyl isocyanate in the solid state (2255 cm^{-1}).[26] On the basis of the ^{11}B NMR spectrum, the purity of the crude isocyanate **7[NEt₄]** was estimated as about 90%.

Initially, we envisioned conversion of isocyante **7[NEt₄]** directly to amine **2**, but this approach was not fruitful. Isocyanate **7[NEt₄]** was insoluble in aqueous HCl even at elevated temperatures. Attempted hydrolysis of **7[NEt₄]** in a 1:1 mixture of 18% HCl and CH_3OH at 80 °C gave a mixture of amine **2** and methyl carbamate **4b[H₃O]** upon extraction from acidified aqueous solutions, according to ^{11}B NMR analysis. The carbamate **4b[H₃O]** was cleanly converted to amine **2** under basic conditions, which prompted us to investigate the carbamates as possible intermediates that could easily be purified and converted to amine **2** in high yields. However, attempts to separate the methyl carbamate **4b[NEt₄]** from carboxylic acid **3[NEt₄]** by chromatography proved difficult due to its low solubility and also an insufficient difference in mobility on silica gel. Therefore, we focused on *t*-Bu carbamate **4a[NEt₄]**, which could be converted to the amine under mildly acidic conditions.

A reaction of isocyanate **7[NEt₄]** with anhydrous *t*-butanol gave carbamate **4a[NEt₄]** in a high yield. Initial attempts at chromatographic separation on a SiO_2 column using CH_3CN/CH_2Cl_2 (1:4) as the eluent showed that pure carbamate **4a[NEt₄]** could be isolated in low yields (~20%). Mass balance was achieved with more polar fractions, which contained mostly amine **2**, apparently arising from deprotection of the BOC group on the SiO_2 support. The decomposition of **4a[NEt₄]** was minimized by buffering the solvent system with 1% NEt_3. The yield of carbamate **4a[NEt₄]** rose to about 50%, but

Scheme 3

8 a: R = OH
b: R = NH₂
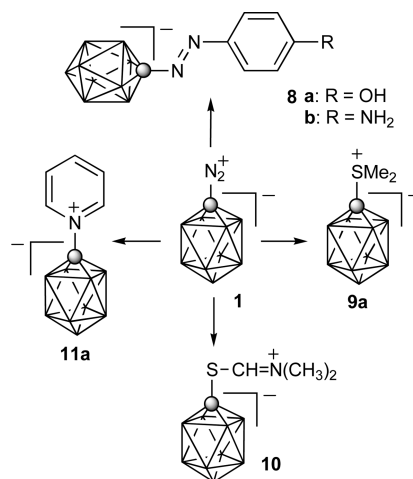
Scheme 4
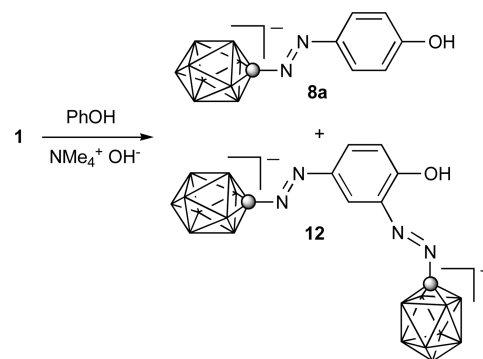
deprotection on the column was still observed. Treatment of carbamate **4a[NEt₄]** with HCl in CH_3OH solution followed by evaporation of the volatiles gave pure **2** in quantitative yield.

Reactivity of [*closo*-1-CB₉H₉-1-N₂]. Dinitrogen derivative **1** was reacted with three types of nucleophiles: activated arenes, divalent sulfur compounds, and pyridine. The reagents were chosen to demonstrate the formation of functionalizable azo derivatives **8** and the formation of inner sulfonium salts directly (**9a**) or through a masked mercaptan (**10**), and to investigate the formation of pyridin-1-yl derivative **11a** (Scheme 3).

A reaction of **1** with stoichiometric amounts of tetraethylammonium phenolate showed that both mono (**8a**) and double (**12**) diazocoupling products were formed in a ratio of up to 5:1 (Scheme 4). Attempts to separate **8a[NEt₄]** from **12[2NEt₄]** were unsuccessful, both by recrystallization (EtOH/H₂O mixtures) and chromatography (CH_3CN/CH_2Cl_2 mixtures). The formation of the double substitution product **12** was minimized by using a 5-fold excess of the phenolate. In contrast, no double diazocoupling was observed in reactions of **1** with stoichiometric amounts of aniline.

Purification of azo derivatives **8a** and **8b** was accomplished by chromatographic separation of the acid extract followed by precipitation as the NMe₄⁺ salt, which gave reasonably pure products in yields of 50% and 80%, respectively. The use of NMe₄⁺ as the counterion gave more crystalline products compared to those with NEt₄⁺.
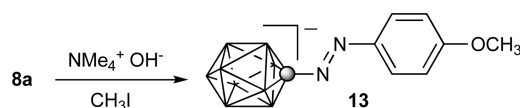
(23) Prakash, G. K. S.; Iyer, P. S.; Arvanaghi, M.; Olah, G. A. *J. Org. Chem.* **1983**, *48*, 3358–3359.
(24) Rawal, V. H.; Zhong, H. M. *Tetrahedron Lett.* **1994**, *35*, 4947–4950.
(25) Laszlo, P.; Polla, E. *Tetrahedron Lett.* **1984**, *25*, 3701–3704.
(26) Paraskewas, S. M.; Danopoulos, A. A. *Synthesis* **1983**, 638–340.

Scheme 5

The azophenol **8a[NMe$_4$]** was easily methylated under basic conditions to give the methoxy derivative **13[NMe$_4$]** in 95% yield (Scheme 5).

Dinitrogen derivative **1** was completely reacted with neat Me$_2$S at ambient temperature over a period of 24 h, giving adduct **9a**, which was isolated in 40% yield. ^{11}B NMR analysis of the crude reaction mixture revealed four signals: three doublets of product **9a** and an unrelated singlet at 20.1 ppm. The singlet appears to be associated with the film of white material, presumably boric acid, which was poorly soluble in CD$_3$CN and well-soluble in CD$_3$OD (18.8 ppm). Previously, **9a** was prepared in 68% yield based on amine **2** without isolation of the intermediate **1**.[12]

A 24 h reaction of **1** with *N,N*-dimethylthioformamide at ambient temperature gave 80% yield of crude **10** after washing with toluene. ^{11}B NMR analysis of the crude product revealed the presence of about 10% of the parent anion [*closo*-1-CB$_9$H$_{10}$]$^-$ (**14**), and also a low intensity singlet at 20.1 ppm. Attempts to purify the zwitterion **10** further were unsuccessful due to its partial decomposition observed during recrystallization from CH$_3$CN/toluene mixtures or 1,2-dichloroethane. Purification on silica gel was avoided, since **10** appeared to be hydrolytically unstable. Alkylation of crude **10** with 1,5-dibromopentane in the presence of a base followed by chromatographic separation and recrystallization gave pure **9b** in 50% yield based on **1** (Scheme 6). This represents a slightly higher yield than that for a single-step preparation of **9a** directly from **1**.

Reactions of **1** with pyridine were most interesting. When **1** was reacted in neat pyridine at ambient temperature for several hours, ^{11}B NMR analysis revealed a complex mixture of at least four products exhibiting characteristic doublets in the region of 25−40 ppm (Table 1). Surprisingly, the major component of the reaction mixture, about 50%, was identified as the 2-isomer **11b[H]**. A doublet at δ 29.6 ppm with 20% intensity was assigned to the parent anion **14** on the basis of a comparison with literature data.[27] This was further supported by a comparison with an authentic sample of **14** with pyridinium as the counterion (**14[PyrH]**) to maintain consistency with the reaction conditions.[28]

The crude mixture was separated on silica gel giving the 2-isomer **11b[H]** in 40% isolated yield as the first fraction. The doublet at δ 35.7 ppm observed in the crude mixture and originally assigned to the B(10) nucleus of **11b** was shifted downfield by about 2 ppm in the isolated sample. This shift presumably results from transformation of the pyridinium salt of **11b[-]** to the zwitterionic structure **11b[H]** of the isolated product. Such downfield shifts were observed for the other two isomers **11c** and **11d**, but they were less significant. The more polar fraction contained a

Scheme 6
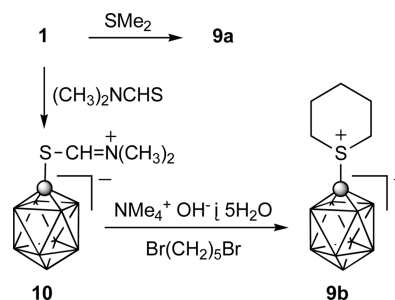
mixture of two other isomers, **11c[H]** and **11d[H]**, which were identified on the basis of 1D ^{1}H and 2D ^{1}H−^{1}H correlation spectroscopy (COSY) NMR analysis.[28]

The addition of hot pyridine to the dinitrogen derivative **1** had a different outcome. ^{11}B NMR analysis of the crude reaction mixture revealed four products [δ B(10): 35.0, 33.1, 31.9, 29.6]. Chromatographic separation gave **11a** in 17% isolated yield as the least polar fraction. The more polar fraction contained the remaining three isomers and also the parent anion **14** in about a 4:4:2:1 ratio (Table 1).

To provide more information about the possible mechanism for the formation of these products, reactions of **1** were run in dilute solutions of pyridine at ambient temperature for 18 h. Thus, a reaction of **1** with a 4% solution of pyridine in CH$_2$Cl$_2$ gave [*closo*-1-CB$_9$H$_9$-1-Cl]$^-$ (**15**)[29] as the major product along with **11a**, **11b**, and **14** in an approximate ratio of 8:3:1:3, respectively, according to the ^{11}B NMR analysis of the crude reaction mixture (Table 1). A similar reaction of **1** with a 4% solution of pyridine in benzene gave [*closo*-1-CB$_9$H$_9$-1-Ph]$^-$ (**16**)[30] as the major product. Isomers **11a** and **11b** were formed as minor products, in 13% and 17% yields, respectively, and no signals belonging to **11c** or **11d** were found in the ^{11}B NMR spectrum of the crude mixture (Table 1). For comparison, decomposition of **1** in pure benzene-d_6 at ambient temperature gave a number of products, among which **16-d_5** was identified by MS. A solution of **1** in CD$_2$Cl$_2$ gave only a broad featureless absorption band in a range −10 to −40 ppm and a broad band around 20 ppm in ^{11}B NMR after 24 h at ambient temperature, which suggests complete destruction of the {*closo*-1-CB$_9$} cluster. Dinitrogen derivative **1** in a 4% solution of pyridine in CD$_3$CN was stable at 0 °C for 3 h, whereas at 45 °C, 45% of **1** reacted in 75 min, giving about 30% **17** (Scheme 7) and 4% **11a** in addition to unidentified signals at 16.7, 25.3, and 10.0 ppm (in decreasing intensity order) in the ^{1}H-decoupled spectrum.

Reaction with MeCN and Kinetic Data for 1. Decomposition of dinitrogen derivative **1** in dried CH$_3$CN at elevated temperatures (∼50 °C) gave a mixture of zwitterion **17** and acetamide **18** in about a 1:1 ratio as the only products (Scheme 7). ^{1}H NMR revealed two partially overlapping quartets centered at 5.91 and 5.52 ppm attributed to **17** and **18**, respectively. Adduct **17** appears to be the primary product, which partially undergoes hydration to the acetamide **18** with residual H$_2$O in the
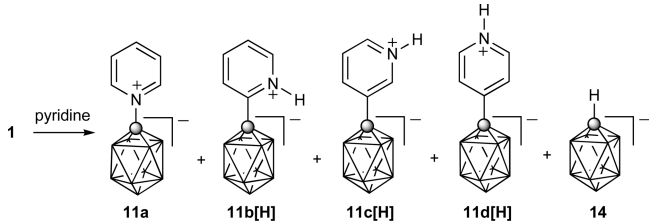
(27) Franken, A.; Kilner, C. A.; Thornton-Pett, M.; Kennedy, J. D. *Inorg. Chem. Commun.* **2002**, *5*, 581–584.

(28) For details, see the Supporting Information.

(29) Ringstrand, B.; Bateman, D.; Shoemaker, R. K.; Janousek, Z. *Collect. Czech. Chem. Commun.* **2009**, *74*, 419–431.

(30) Jelinek, T.; Kilner, C. A.; Thornton-Pett, M.; Kennedy, J. D. *Chem. Commun.* **2001**, 1790–1791.

Table 1. Product Distributions in Reaction of **1** with Pyridine

condition\products	**11a**	**11b[H]**	**11c[H]**	**11d[H]**	**14**
			Neat Pyridine		
25 °C[a]	traces	40%[b]	17%[c]	10%[c]	6%[c]
90 °C[c]	17%[b]	20%[c]	18%[c]	9%[c]	5%[c]
			Solutions of Pyridine		
4% in CH_2Cl_2[d]	17%[e]	7%[e]	0%[e]	0%[e]	20%[e]
4% in benzene[f]	13%[e]	17%[e]	0%[e]	0%[e]	5%[e]
^{11}B NMR for B(10), δ[g]	33.1 ppm	37.2 ppm	33.9 ppm	35.9 ppm	29.6 ppm

[a] About 75% of total mass recovery after separation on SiO_2. [b] Yield of isolated product. [c] Yield based on ^{11}B NMR of the mixture corrected for its mass. [d] [*closo*-1-CB_9H_9-1-Cl]⁻ (**15**) constituted 56% of the mixture. [e] Ratio of low field signals for the crude reaction mixture. [f] [*closo*-1-CB_9H_9-1-Ph] (**16**) constituted 65% of the crude reaction mixture. [g] Chemical shifts of the isolated products or mixtures.

Scheme 7
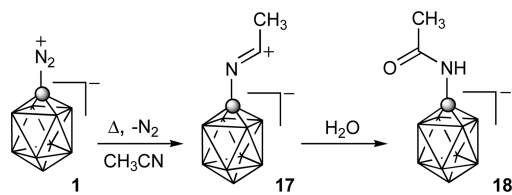
solvent. Exposure of the crude reaction mixture to moisture quickly and quantitatively converted **17** to the acetamide **18**, which was isolated and characterized by NMR and MS techniques. The clean transformation of **1** to the two related products and sufficient separation of the signals in the ¹H NMR spectrum made it possible to analyze kinetics of this reaction. It is believed that the rate-determining step of the process is the heterolytic cleavage of the C—N bond in **1**.

The kinetics of decomposition of the dinitrogen derivative **1** were investigated in dried CD_3CN as a function of the temperature and were followed by ¹H NMR spectroscopy. Intensities of the disappearing B(10)-**H** signal at 7.21 ppm, which is part of a quartet centered at 6.72 ppm belonging to **1**, and the growing peak at 5.82 ppm, part of the pseudo quintet (partially overlapping quartets of **17-d_3** and **18-d_3**), were used to calculate the ratio of **1** to the sum of products **17-d_3** and **18-d_3**. Standard kinetic analysis using the Erying equation found $\triangle H^{\ddagger} = 38.4 \pm 0.8$ kcal mol⁻¹, $\triangle S^{\ddagger} = 44.5 \pm 2.5$ cal mol⁻¹ K⁻¹, and $\triangle G^{\ddagger} = 25.1 \pm 0.8$ kcal mol⁻¹ at 298 K.[28]

Mechanistic Studies. Computational Analysis. To shed more light on properties of **1** and its reactions with nucleophiles, we conducted quantum-mechanical calculations initially at the B3LYP/6-31G(d,p) level of theory to establish conformational minima and to obtain thermodynamic corrections. The resulting structures were used to calculate the self-consistent field (SCF) energies at the MP2/6-31G(d,p) level of theory. Since **1** and other molecules involved are highly polar or ionic, the SCRF
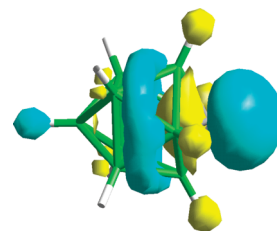

Figure 2. The MP2/6-31G(d,p) derived contour for the LUMO ($E = -1.57$ eV) of ylide **19**.

solvation model was used to compute their SCF energies at the MP2/6-31G(d,p) or MP2/6-31+G(d,p) level of theory in an appropriate dielectric medium (pyridine or MeCN). Computational results are shown in Figures 2—6 and Tables 2—7, and full numerical data are provided in the Supporting Information.[28]

Generation and Structure of the Carbonium Ylide 19. The dinitrogen derivative **1** undergoes a heterolytic cleavage of the C_{cage}—N bond, and the process is calculated to be endothermic by 33.2 kcal/mol in the gas phase at the MP2//DFT level of theory with the 6-31G(d,p) basis set. This value is practically the same as that obtained using the MP2//MP2 method with the same basis set (Table 2). Since the resulting carbonium ylide **19** ($\mu = 4.0$ D) is less polar than **1** ($\mu = 6.1$ D), the endotherm increases to 35.4 kcal/mol in pyridine ($\varepsilon = 13.3$) and to 36.4 kcal/mol in the MeCN ($\varepsilon = 36.6$) dielectric medium. The MP2//DFT and MP2//MP2 calculations using diffuse functions do not change the results significantly, although they give lower ΔH values up to 2 kcal/mol for the latter method. In contrast to the MP2 results, the enthalpy change in the reaction calculated by the DFT method was smaller by about 10 kcal/mol. This difference is related to the inadequate treatment of electron correlation by the DFT methods and demonstrates the importance of dispersive forces in the stabilization of **1**.

A transition state search with the DFT method for the loss of N_2 by **1** located a transition structure, **1-TS**, in
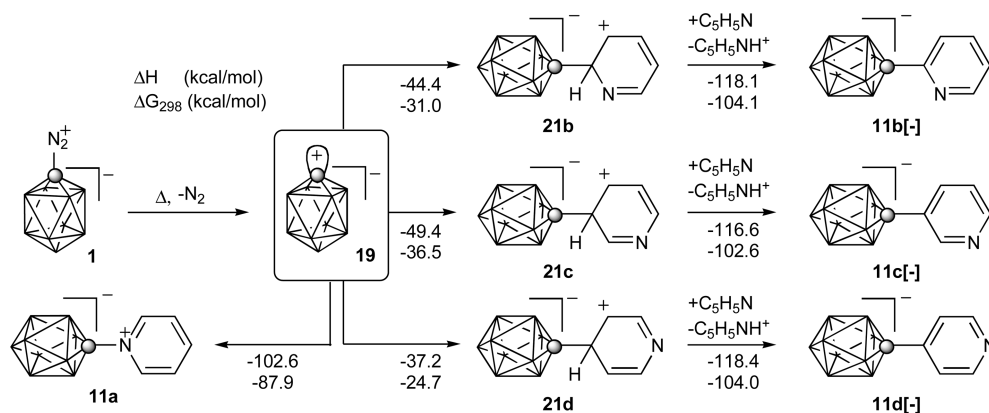
Figure 3. Electrophilic substitution of pyridine. Energy change relative to ylide **19** and pyridine (MP2/6-31G(d,p)//B3LYP/6-31G(d,p), $\varepsilon = 13.3$). For the reaction with radical ion **26**, the intermediates **28** are analogous to **21** with the delocalized unpaired spin instead of the positive charge.
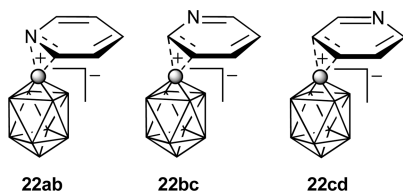

Figure 4. Structures of the edge adducts of **19** to pyridine.

which the $C_{cage}-N$ bond is elongated by about 0.8 Å (d_{C-N} = 2.13 Å). The DFT calculated activation parameters, $\Delta H^{\ddagger} = 25.4$ kcal/mol and $\Delta S^{\ddagger} = 12.5$ cal/(mol K), fall short of the experimental data (vide supra). Single-point calculations for **1-TS** at the MP2//DFT level of theory gave $\Delta H^{\ddagger} = 30.4$ kcal/mol in the pyridine dielectric medium, which is lower by 6 kcal/mol than the enthalpy change for the complete reaction. In addition, the calculations closely approximated an energy plateau between $d_{C-N} = 2.13$ Å ($\Delta E_{SCF} = 33.95$ kcal/mol) and $d_{C-N} = 2.70$ Å ($\Delta E_{SCF} = 34.45$ kcal/mol), whereas ΔE_{SCF} for $d_{C-N} = 3.5$ Å is 36.6 kcal/mol and for the complete reaction is 37.8 kcal/mol.

MP2-level calculations demonstrated that the carbonium ylide **19**, a member of a *hypercloso* family, is a zwitterionic species. The carbon exocyclic (radial) orbital is practically a pure p orbital and partially populated (−0.34 e) at the expense of the boron atoms in the lower belt (Table 3). The lowest unoccupied molecular orbital (LUMO) of **19** is primarily localized on the C_{cage} atom with a contribution from the lower belt of boron atoms (Figure 2).

The loss of electron density from the carbon exocyclic orbital markedly affects the geometry of the {*closo*-1-CB_9} cage (Table 3). Thus, the departure of N_2 from **1** results in a less pyramidalized apical carbon atom, contraction of the $C_{cage}-B$ interatomic distances, and significant expansion of the interbelt B−B bonds in the ylide **19** as compared to **1**.

Electronic and geometrical features of **19** are similar to those found for its recently reported and extensively discussed 12-vertex *B*-undecamethyl analogue, the [*closo*-1-CB_{11}Me_{11}] ylide.[31]

Reaction of Ylide 19 with Nucleophiles. The resulting electron-deficient intermediate, carbonium ylide **19**, is a

(31) Vyakaranam, K.; Korbe, S.; Divisova, H.; Michl, J. *J. Am. Chem. Soc.* **2004**, *126*, 15795–15801.

highly reactive electrophile. In the simplest case, it reacts with Lewis bases in a two-electron process, giving C-substitution products such as **9**, **11a**, and **20**. The overall two-step nucleophilic substitution reactions (S_N1) of **1** are highly exothermic, with the enthalpy change exceeding −30 kcal/mol and typically about −60 kcal/mol in a vacuum (Table 4). Analysis of the results for the four isomeric pyridine adducts **11a[H]**−**11d[H]** demonstrates that the most thermodynamically stable isomer is **11b[H]**, while the least stable is the *N*-isomer **11a** (**11b[H]** > **11d[H]** > **11c[H]** > **11a**) in a vacuum. The compounds have substantial dipole moments, up to 3 times that for the starting dinitrogen derivative **1** (6.1 D), and a significant solvent effect on the reaction's exotherm can be expected in polar media. Indeed, isodensity polarizable continuum model (IPCM) calculations in the dielectric medium increase the stability of all isomers, but the largest gain is observed for the C(3)-isomer **11c[H]**. Consequently, the ΔH for the formation of **11c[H]** in pyridine solutions is about 21 kcal/mol larger than in a vacuum, which makes it the most exothermic and exoergic process among the formations of all regioisomers (Table 4). The exotherm for the formations of other regioisomers are smaller, and the resulting order of thermodynamic stability follows: **11c[H]** > **11b[H]** > **11d[H]** > **11a**. Interestingly, in both sets of calculations, the *N*-isomer **11a** is predicted to be the least thermodynamically stable.

MP2//DFT calculations demonstrated that the dipole moment of the zwitterionic compounds significantly depends on the solvent polarity (Table 4). For instance, with increasing polarity of the medium, the dipole moment of **1** increases ($\mu = 6.1$ D, $\varepsilon = 1$; $\mu = 8.1$ D, $\varepsilon = 13.3$; $\mu = 8.4$ D, $\varepsilon = 36.6$) due to increasing negative charge at the 10 position from +0.062 for B(10) and +0.0013 for H(10) ($\varepsilon = 13.3$) to +0.051 for B(10) and −0.0002 for H(10) ($\varepsilon = 36.6$). This is consistent with the observed solvent effect on NMR spectra and higher nuclear shielding of these atoms in CD_3CN as compared to benzene-d_6 solutions (vide supra).

Calculations in the dielectric medium also demonstrated that two of the protonated derivatives, **11b[H]** and **11d[H]**, are significantly stronger acids than pyridinium, and proton transfer to pyridine is moderately exothermic (Table 5). For the C(3) isomer **11c[H]**, the process is practically thermoneutral. The resulting anions **11[-]** have very similar energies in the pyridine dielectric medium, with the C(4) isomer **11d[-]** slightly more stable
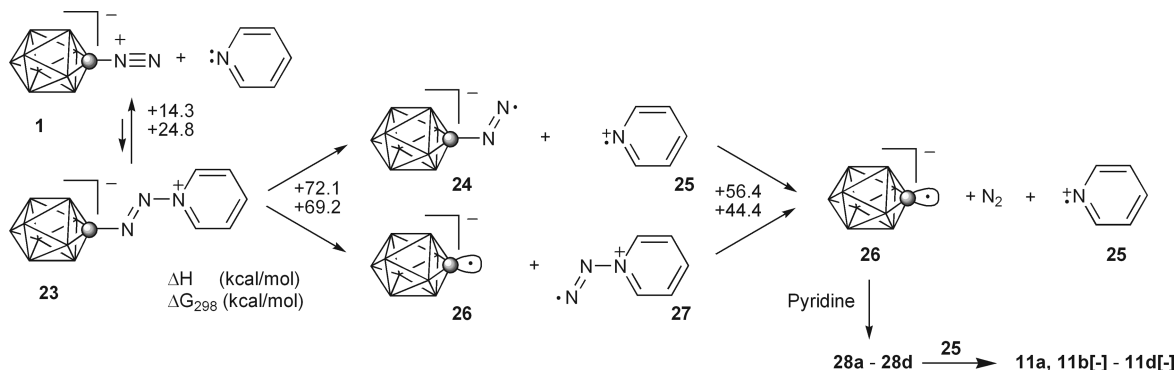
Figure 5. Formation of radical ion **26**. Enthalpy change relative to **1** and pyridine reactants calculated with MP2/6-31G(d,p)//B3LYP/6-31G(d,p) for the pyridine solution ($\varepsilon = 13.3$).

Table 2. Enthalpy Change in Heterolytic Dissociation of **1**[a]

method	ΔH, kcal/mol
Gas Phase	
B3LYP/6-31G(d,p)	24.6
MP2/6-31G(d,p)//B3LYP/6-31G(d,p)	33.2
MP2/6-31G(d,p)	33.3
ICPM model ($\varepsilon = 36.6$)	
MP2/6-31G(d,p)//B3LYP/6-31G(d,p)	36.4
MP2/6-31+G(d,p)//B3LYP/6-31G(d,p)	35.0
MP2/6-31+G(d,p)//MP2/6-31G(d,p)	34.4

[a] B3LYP/6-31G(d,p) thermodynamic corrections. $\Delta S = +43.6$ cal/molK.

Table 3. Calculated Structural Parameters for Selected Derivatives of {*closo*-1-CB$_9$}

	X = H	X = N$_2^+$	X = •	X = +
	14	**1**	**25**	**19**
	Geometry[a,b]			
C(1)−B(2)/Å	1.602	1.624	1.585	1.532
B(2)−B(3)/Å	1.836	1.885	1.849	1.928
B(2)−B(6)/Å	1.802	1.785	1.809	1.829
B(6)−B(10)/Å	1.700	1.711	1.698	1.678
B−C−B/deg	108.3	110.2	111.2	125.8
	Natural Atomic Charge[c]			
C(1)	−0.77	−0.52	−0.36	−0.34
B(2)	0.03	0.08	−0.01	0.07
B(6)	−0.19	−0.19	−0.18	0.11
B(10)	−0.17	−0.06	−0.20	−0.32
	Bonding[c]			
C(1) exo	sp$^{2.03}$ (1.94)	sp$^{3.37}$ (1.96)	sp$^{3.97}$ (0.95)	sp$^{99.8}$ (0.67)

[a] Optimized at the MP2/6-31G(d,p) level of theory at the C_{4v} point group symmetry. [b] C_{cage}−N distance, 1.337 Å; N−N distance, 1.149 Å. [c] NBO analysis. Exocage orbital occupancy in parentheses.

than the C(2) isomer **11b[-]** and more stable by 1.7 kcal/mol than **11c[-]**.

Formation of Pyridine Derivatives 11. The formation of four regioisomeric products, **11a**−**11d**, may involve either a two-electron or a one-electron process. Initially, we focused on the former and considered electrophilic reactions of the carbonium ylide **19** with pyridine.

The formation of the N(1) isomer (**11a**) can be envisioned as a simple one-step collapse of a Lewis acid (ylide **19**) and a Lewis base (pyridine) to form the C$_{cage}$−N bond (Figure 3). Our attempts to locate the transition state for the reaction using the DFT method were unsuccessful, which indicates that the process may be practically barrierless. In contrast, the formation of the C-substituted isomers **11b**−**11d** involves a two-step process, with the initial formation of arenium zwitterions **21b**−**21d** followed by a proton transfer. The calculated energy for the arenium ions is much higher, by about 60 kcal/mol, than that for the direct adduct **11a**. Computational results indicate that the order of stability for zwitterions **21** follows **21c** > **21b** > **21d** in both the gas phase and the dielectric medium; the latter stabilizes the highly polar intermediates by 10−13 kcal/mol relative to the gas phase. Proton transfer from **21** to pyridine and the formation of anions **11[-]** are highly exothermic, which

renders the process irreversible. The computational result favoring the C(3) isomer **21c** is consistent with the established regioselectivity of electrophilic substitution in pyridine[32] but is not consistent with the experimental observation of formation of the C(2) regioisomer **11b** as the major product.
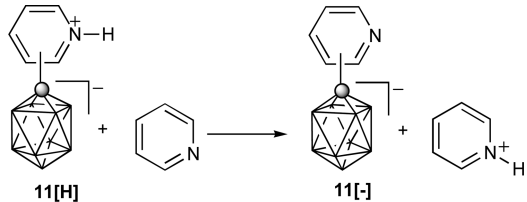
Full structure optimizations at the MP2/6-31G(d,p) level of theory gave a different geometry for the intermediate complex of ylide **19** with pyridine (Figure 4). Instead of a Wheland-type adduct, in which the {1-*closo*-CB$_9$} cluster is connected to the arenium fragment by a single bond about 1.60 Å long (**21**, Figure 3), the MP2-optimized geometry shows adduction to an edge (C=C bond) of the aromatic ring forming a three-center, two-electron bond in **22bc** and **22cd** (Figure 4). Attempts at

(32) Eicher, T.; Hauptmann, S. In *The Chemistry of Heterocycles*; Georg Thieme Verlag: New York, 1995; pp 273−276 and references therein.

Table 4. Enthalpy Change in Substitution Reactions of **1**[a]

reagent	product	X	ΔH/kcal mol^{-1}		dipole/D	
			$\varepsilon = 1$[b]	$\varepsilon = 13.3$[c]	$\varepsilon = 1$[b]	$\varepsilon = 13.3$[c]
Me$_2$S	**9a**	Me$_2$S$^+$	−45.5	[d]	12.8	[d]
pyridine	**11a**	1-C$_5$H$_5$N$^+$	−59.2	−67.2	15.1	18.6
	11b[H]	2-C$_5$H$_4$NH$^+$	−67.9	−76.4	15.7	19.1
	11c[H]	3-C$_5$H$_4$NH$^+$	−59.9	−81.4	19.2	24.2
	11d[H]	4-C$_5$H$_4$NH$^+$	−61.0	−75.4	19.2	24.2
MeCN	**17**	MeCN$^+$	−30.7	−34.7[e]	14.0	17.4[e]
NMe$_3$	**20**	NMe$_3$$^+$	−60.0	[d]	13.3	[d]

[a] MP2/6-31G(d,p)//B3LYP/6-31G(d,p) level with DFT thermodynamic corrections. [b] Vacuum calculations. [c] IPCM solvation model. [d] Not calculated. [e] Calculated for $\varepsilon = 36.6$.

Table 5. Calculated Free Energy Change in Deprotonation Reactions of **11**[a]

	b	**c**	**d**
ΔG_{298} kcal mol^{-1}	−5.9	+0.5	−7.3

[a] MP2/6-31G(d,p)//B3LYP/6-31G(d,p) calculations with DFT thermodynamic corrections. IPCM solvation model $\varepsilon = 13.3$.

obtaining equilibrium geometry for the analogous structure **22ab**, with the C$_{cage}\cdots$C$\cdots$N two-electron bond, were unsuccessful, and the optimization gave the structure of **11a** instead. Geometry reoptimization at the DFT level of theory starting at the **22bc** geometry resulted in the structure **21b**. The C$_{cage}$−C$_{ring}$ distances in **22bc** (adduct to the C(2)−C(3) edge) and **22cd** (adduct to the C(3)−C(4) edge) are about 1.7 Å. Subsequent deprotonation of **22** leads to the formation of the product **11**. MP2 results demonstrated that both complexes have similar energies ($\Delta E_{SCF} = 2.0$ kcal/mol), which are comparable to those of the Wheland complexes **21**.

Structures similar to those of **22** were deduced from experimental data for intermediates involved in reactions of [*hypercloso*-1-CB$_{11}$Me$_{11}$] ylide with aromatic hydrocarbons.[33]

Even though transition state structures for the formation of **21** and **22** were not located and their energies were not calculated, it seems unlikely that **21** and **22** would be formed preferentially to the direct collapse of the reactants into the N(1) isomer **11a**. Indeed, a reaction of [*hypercloso*-1-CB$_{11}$Me$_{11}$] ylide with pyridine gives the corresponding N(1) isomer as the only isolated product.[33]

(33) Vyakaranam, K.; Havlas, Z.; Michl, J. *J. Am. Chem. Soc.* **2007**, *129*, 4172–4174.

An alternative mechanism for the formation of **11b**−**11d** may involve a radical process initiated by the addition of pyridine to the electrophilic dinitrogen group of **1**. Indeed, both DFT- and MP2-level calculations located the pyridine adduct **23** on the potential energy surface (PES). The formation of the highly polar azene **23** ($\mu = 23.2$ D) was found to be endothermic by 14.3 kcal/mol or endoergic by 24.8 kcal/mol at the MP2//DFT level of theory in the pyridine dielectric medium ($\varepsilon = 13.3$).

According to this mechanism, azene **23** undergoes fragmentation with a homolytic cleavage of the N−pyridine bond, leading to the radical ion pair **24** and **25** (Figure 5). The process is highly endothermic in the gas phase ($\Delta H = 133.0$ kcal/mol), but it becomes more favorable in the pyridine dielectric medium ($\Delta G_{298} = +44.5$ kcal/mol). The diazenyl radical **24** easily loses molecular nitrogen ($\Delta G_{298} = -24.8$ kcal/mol) and forms radical ion **26**. The dissociation of the C$_{cage}$−N bond and the direct formation of radical anion **26** is also possible, although the second ion, the pyridinediazenyl radical (**27**), was not located on the potential energy surface with the DFT method. The calculated overall enthalpy change for the formation of the ion pair and N$_2$ from **1** is +145.9 kcal/mol in the gas phase, but in pyridine ($\varepsilon = 13.3$), this energy is lowered to $\Delta H = 56.4$ kcal/mol or $\Delta G_{298} = 44.4$ kcal/mol (Figure 5).
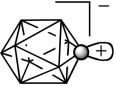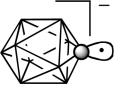
NBO analysis indicates that the apical carbon atom in radical ion **26** has a significant negative charge density (−0.36) and the radical is expected to be moderately nucleophilic (Table 3). Therefore, it may react with a molecule of neutral pyridine (solvent), which leads to regioisomeric radical anion adducts **28** (analogous to zwitterions **21** in Figure 3). Results show that, in the gas phase, the C(2) intermediate **28b**, which leads to the experimentally observed major product **11b**, is least favored, and its regioisomers are more stable by about 3−4 kcal/mol (stability order: **28c** > **28a**, **28d** > **28b**, Table 6). The IPCM calculations demonstrated diminished exotherms of the adduct formation in the dielectric medium, with the heat of formation for the C(2) adduct **28b** being least affected. Consequently, the order of stability of the intermediates is changed in pyridine; the N(1) adduct **28a**, leading to the unobserved **11a**, becomes the least favored, whereas **28b** is less stable than **28c** by only 1.4 kcal/mol (order of stability: **28c** > **28b** > **28d** > **28a**, Table 6). The resulting adducts **28b**−**28d** undergo a highly exothermic (about 115 kcal/mol) process, leading to products **11b[-]**−**11d[-]** and involving either a hydrogen atom transfer or a sequence of electrons followed by proton transfer with pyridinium radical **25**. A reaction of radical anion **26** with pyridine radical cation **25** is predicted to be highly exothermic and lead directly to **11a**.

Our initial attempts to locate transition state structures for either type of adduct, radicals **28** or zwitterions **21**, were unsuccessful and, due to computational intensity, were not pursued further.

Phenylation of Pyridine. To provide a better support for the proposed radical process of formation of **11**, we also analyzed an analogous reaction between the benzenediazonium ion and pyridine (Figure 6 and Table 6). According to the accepted mechanism, the formation of

Table 6. Calculated Enthalpy Change for Reactions with Pyridine[a]

reaction intermediate				N(1)	C(2)	C(3)	C(4)
R*	*	adduct	ε	a	b	c	d
19	+	**21**	1^b	−92.5	−32.0	−36.4	−26.9
			13.3^c	−102.6	−44.4	−49.4	−37.2
26	•	**28**	1^b	−28.0	−24.9	−29.2	−28.0
			13.3^c	−22.9	−23.4	−24.8	−23.1
$C_6H_5^{\bullet}$ **32**	•	**33**	1^b	−28.4	−26.0	−27.6	−25.8
			13.3^c	−26.0	−25.3	−28.4	−28.0

[a] MP2/6-31G(d,p)//B3LYP/6-31G(d,p) level with DFT thermodynamic corrections. [b] Vacuum calculations. [c] IPCM solvation model.

N-phenylazopyridinium (**29**) is the first step in the free radical phenylation of pyridine, which leads to three regioisomeric *C*-phenylpyridines (**30**).[34−36] DFT calculations located the *N*-diazene **29** on the potential energy surface, and subsequent MP2//DFT calculations revealed that its formation is moderately endothermic ($\Delta H =$ +2.9 kcal/mol, ΔG_{298} = +14.5 kcal/mol) in the pyridine dielectric medium (Figure 6). Homolytic cleavage of the N−N bond leading to the formation of phenyldiazenyl radical (**31**) and radical cation **25** is significantly endoergic (ΔG_{298} = +51.7 kcal/mol). This is partially compensated by the favorable decomposition of the diazenyl radical **31** and the formation of phenyl radical (**32**) and N$_2$ (ΔH = −11.6 kcal/mol, ΔG_{298} = −21.5 kcal/mol). Nevertheless, the overall process of formation of the phenyl radical is endothermic (Figure 6).

The addition of the resulting phenyl radical (**32**) to pyridine and the formation of the intermediates **33** is moderately exothermic with the highest exotherm calculated for the *N*-adduct **33a** (stability order: **33a** > **33c** > **33b** > **33d**) in the gas phase (Table 6). The same calculations in the dielectric medium decrease the reaction exotherm for **33a** and **33b** and increase the exotherm for **33c** and **33d**. Consequently, the order of thermodynamic stability of the four intermediates is altered, giving the preference for the C(3) isomer **33c** (stability order: **33c** > **33d** > **33a** > **33b**) in pyridine. Subsequent H• transfer from **33** to **25** is highly exothermic ($\Delta H \approx$ −110 kcal/mol) and gives the isomeric pyridines **30**. The calculated order of their thermodynamic stability (**30b** > **30d** $\sim$ **30c**) is consistent with experimentally established trends in heats of formation.[37]

Finally, we assessed the accuracy of the IPCM method in predicting the formation of ion pairs, such as **25** and **26**,
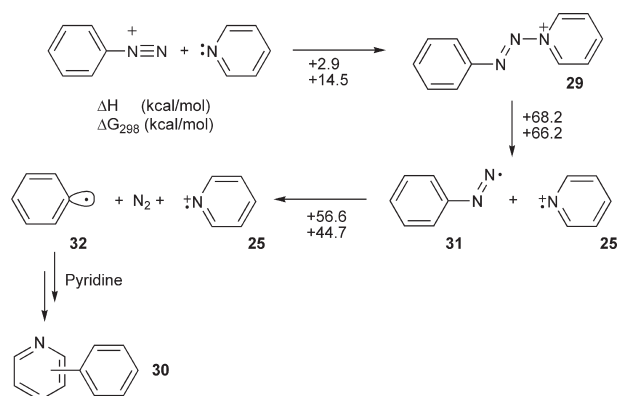
Figure 6. Formation of phenyl radical **32**. Energy change relative to initial reactants calculated with MP2/6-31G(d,p)//B3LYP/6-31G(d,p) for the pyridine solution ($\varepsilon = 13.3$).

Table 7. Energy Change in Dissociation of **34** in MeOH[a]

ε	ΔH/kcal mol^{-1}	ΔG_{302}/kcal mol^{-1}
1^b	67.9	56.1
$30.9^{c,d}$	24.5	12.6

[a] MP2/6-31G(d,p)//B3LYP/6-31G(d,p) level with DFT thermodynamic corrections. [b] Vacuum calculations. [c] IPCM solvation model. [d] Value interpolated from data in ref 39.

by computing of the energy change for dissociation of azosulfone **34** and the formation of ion pair PhN$_2^+$ and PhSO$_2^-$ in a dielectric medium. The experimentally[38] established association constant $K_{assoc} = 1.44 \times 10^5$ L/mol for the ion pair PhN$_2^+$ and PhSO$_2^-$ in MeOH at 29 °C allows for the calculation of $\Delta G_{302} = +7.1$ kcal/mol

(34) Abramovitch, R. A.; Saha, J. G. *Tetrahedron* **1965**, *21*, 3297–3303.
(35) Zollinger, H. *Acc. Chem. Res.* **1973**, *6*, 335–341.
(36) Galli, C. *Chem. Rev.* **1988**, *88*, 765–792.
(37) Ribeiro da Silva, M. A. V.; Matos, M. A. R.; Rio, C. A.; Morais, V. M. F.; Wang, J.; Nichols, G.; Chickos, J. S. *J. Phys. Chem. A* **2000**, *104*, 1774–1778.
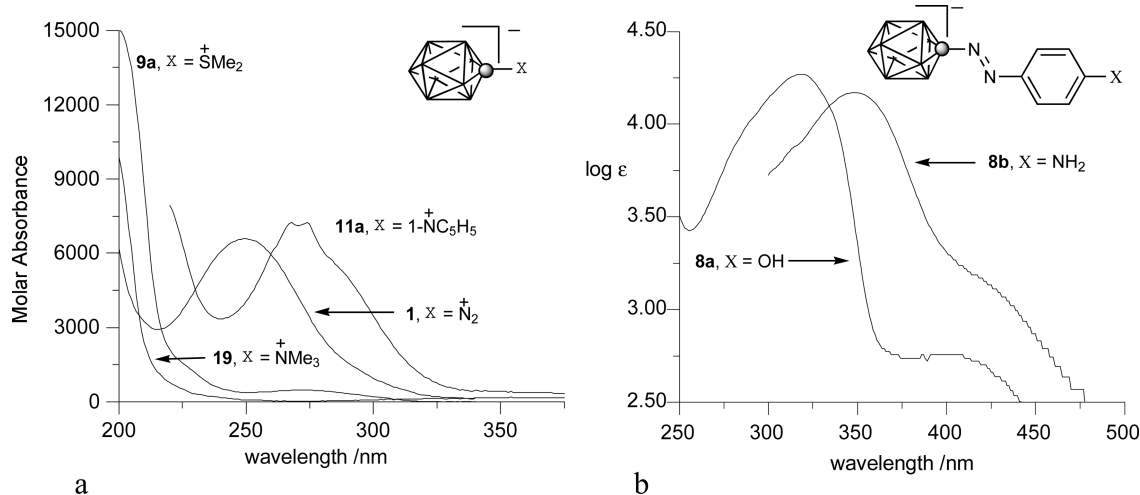
(38) Ritchie, C. D.; Saltiel, J. D.; Lewis, E. S. *J. Am. Chem. Soc.* **1961**, *83*, 4601–4605.

Figure 7. Electronic absorption spectra for selected compounds recorded in CH$_3$CN.
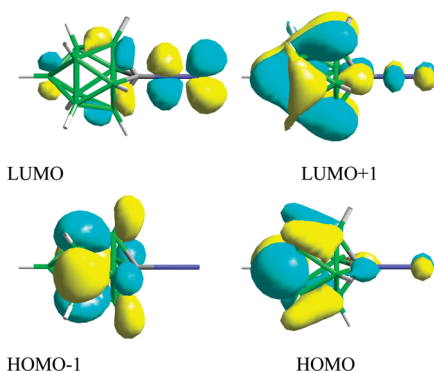
Figure 8. DFT-generated MO contours for **1**. For clarity, only one part of each degenerated MO is shown.

Figure 9. DFT-generated HOMO and LUMO contours for **11a**.
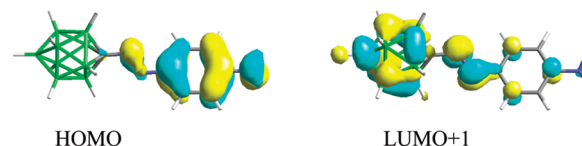
Figure 10. ZINDO-generated HOMO and LUMO+1 contours for **8b**.

for the dissociation of **34**. Our MP2//DFT calculations in the gas phase demonstrated a high endotherm (ΔH = +67.9 kcal/mol) for the dissociation process of **34** (Table 7). In the dielectric medium, however, the dissociation process of **34** becomes significantly more favorable, reaching a value of $\Delta G_{302} = +12.6$ kcal/mol in MeOH. This represents a fairly good agreement between the theory and experimental results and indicates that MP2//DFT calculations underestimated the solvation of the ions by 5.5 kcal/mol. Consequently, the stability of other ions in a dielectric medium is most likely underestimated, and their formation is more favorable than calculated.

Electronic Absorption Spectroscopy. Spectroscopic analysis of four derivatives, **1**, **8**, **9a**, **11a**, and trimethylamine zwitterion **20** provides a convenient means to study electronic interactions between the {*closo*-1-CB$_9$} cage and the substituent at the C(1) position.

Among the five substituents, NMe$_3$ in **20** is the simplest and does not possess easily available electrons or accessible orbitals. Therefore, the electronic absorption spectrum of **20** closely resembles that of the parent [*closo*-1-CB$_9$H$_{10}$]$^-$ anion (**14**) with the absorption tailing to about 250 nm and the maximum below 200 nm (Figure 7a). The presence of an electron pair in the SMe$_2$ substituent of **9a** resulted in the increased intensity of the band at about 200, the appearance of a shoulder band at about 225 nm, and also a broad low-intensity band at 272 nm.
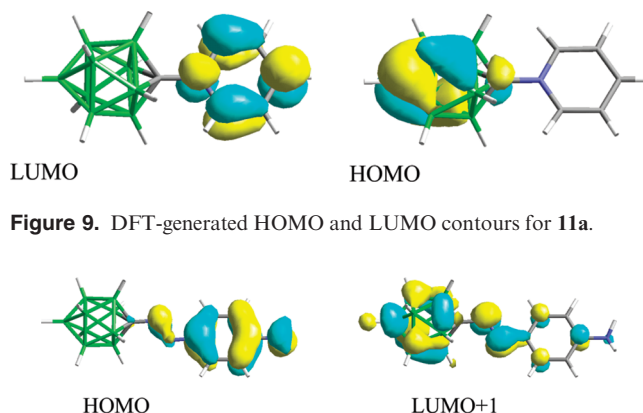
These spectral features are consistent with the transitions observed at about 230 and 200 nm for trialkylsulfonium salts.[40] It was also noted that the UV spectra of sulfonium salts are affected by the presence of molecular oxygen, which gives rise to the appearance of charge-transfer (CT) bands.[40]

The dinitrogen, N$_2$, and pyridine groups are π substituents, and their orbitals can interact with the electronic manifold of the {*closo*-1-CB$_9$} cage. Thus, the dinitrogen derivative **1** exhibits a single absorption band at 250 nm (Figure 7a). ZINDO//MP2 calculations revealed that **1** exhibits two $\pi \rightarrow \pi^*$ transitions, at 280 nm ($f = 0.49$) and a weaker one at 242 nm ($f = 0.12$) in a vacuum. The former involves the double-degenerated highest occupied molecular orbital (HOMO), localized mostly on the cage, and the LUMO, localized primarily on the N$_2$ group (Figure 8). The higher energy transition is due to intracage excitations (HOMO $\rightarrow$ LUMO+1). The same calculations conducted for **1** in the dielectric medium of the solvent ($\varepsilon = 36.6$) revealed a substantial negative solvatochromic effect of the cage-to-substituent excitation and practically no solvent effect of the intracage excitation. As a consequence, the two transitions merge into one, which is calculated at 247 nm ($f = 0.56$) and observed at 250 nm.

(39) Le Fèvre, R. J. W. *Trans. Faraday Soc.* **1938**, *34*, 1127–1132.
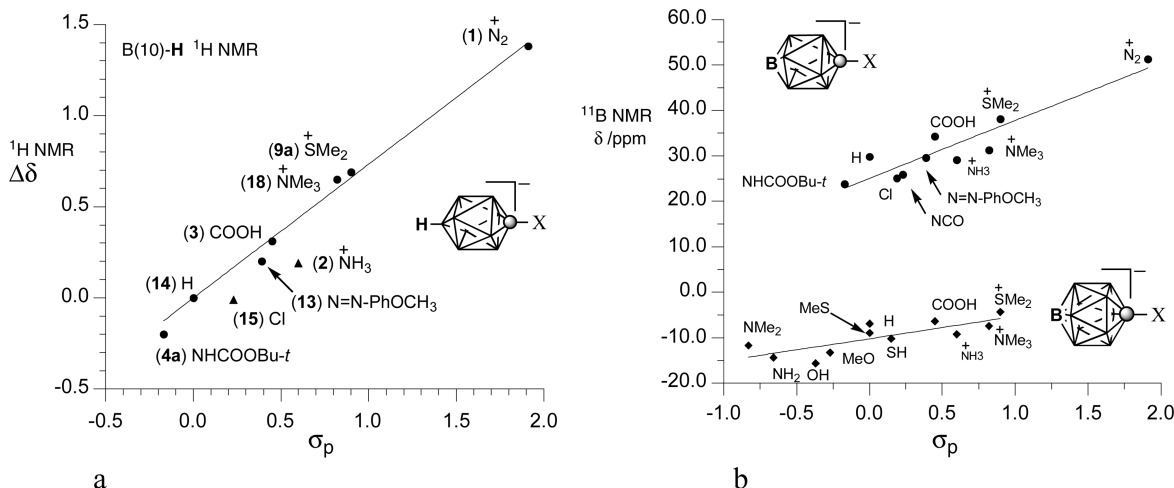(40) Ohkubo, K.; Yamabe, T. *J. Org. Chem.* **1971**, *36*, 3149–3155.

Figure 11. Relative ^{1}H (a) and absolute ^{11}B (b) NMR chemical shifts measured in CD$_3$CN for the antipodal position of [*closo*-1-CB$_9$H$_9$-1-X]$^-$ and [*closo*-1-CB$_{11}$H$_{11}$-1-X]$^-$ plotted against the substituent σ_P values. The σ_P parameters of the $-$N$=$N$-$Ph and $-$NHCOOMe groups were used for the substituents in **13** and **4a**, respectively. Best fit lines: (a) $y = 0.73x$, $r^2 = 0.990$; (b) {*closo*-1-CB$_9$} $y = 12.7x + 25.1$, $r^2 = 0.86$; {*closo*-1-CB$_{11}$} $y = 5.3x - 10.0$, $r^2 = 0.67$.

Pyridine is the most complex substituent among the five groups; it has both the low-lying LUMO and also its own $\pi \rightarrow \pi^*$ transitions in the UV region. Consequently, the pyridine derivative **11a** is expected to exhibit three types electronic transitions: cage-ring, intraring, and intracage. The first two types apparently overlap and form a complex structure in the range of 240−300 nm (Figure 7a). The maximum of the broad, intense underlying band is estimated at 269 nm and attributed to the cage-to-ring CT transition. The upper fine structure has two maxima at 268 and 274 nm and represents the pyridine B-band. Results of ZINDO//MP2 calculation for **11a** in a dielectric medium ($\varepsilon = 36.6$) support this assignment. The CT transition is calculated at 260 nm ($f = 0.32$) and involves the HOMO $\rightarrow$ LUMO excitation (Figure 9) with a small contribution from the intracage excitation (HOMO $\rightarrow$ LUMO+4). The pyridine B-band appears at 272 nm ($f = 0.08$) and involves HOMO−2 $\rightarrow$ LUMO excitation. The same calculations for **11a** in a vacuum give the CT transition at 361 nm ($f = 0.18$), which demonstrates a large negative solvatochromic effect (-1.34 eV) in this polar derivative (Table 4). The pyridine B-band experiences a smaller and positive solvatochromic shift ($+0.37$ eV).

Electronic spectra of the azo derivatives **8a** and **8b** exhibit absorption bands typical for azobenzenes.[41] The intense band of the $\pi \rightarrow \pi^*$ transition in azophenol **8a** appears at 318 nm (log $\varepsilon = 4.30$) and in azoaniline **8b** at 348 nm (Figure 7b), while the forbidden $n \rightarrow \pi^*$ transition is located at about 400 nm in both derivatives.

ZINDO//DFT calculations in the MeCN dielectric medium ($\varepsilon = 36.6$) demonstrated a low-intensity transition at 445 nm ($f < 0.001$), which involves excitation from HOMO−2 and HOMO−4, localized on the nitrogen atom lone pairs and the cage, to the π symmetry orbitals LUMO$+1$ and LUMO$+4$, which are delocalized over the molecule with the main component from the {*closo*-1-CB$_9$} cage. The more intense transition is calculated at 329 nm ($f = 0.82$), which involves the excitation from the

HOMO, localized on the organic fragment, mainly to the LUMO$+1$ and also to the LUMO$+4$ localized on the CB$_9$H$_9-$N$=$N fragment (Figure 10).

In comparison to the azobenzene analogs, the electronic transitions of the {*closo*-1-CB$_9$} derivatives **8a** and **8b** are blue-shifted by 24−34 nm. For instance, absorption bands of 4-hydroxyazobenzene are recorded at 344 and 425 nm in CH$_3$CN.[42] In 4-aminoazobenzene, both absorption bands overlap to form a broad band[43] with a maximum at 382 nm in CH$_3$CN.[44]

NMR Studies. The availability of several diverse derivatives of the [*closo*-1-CB$_9$H$_{10}$]$^-$ cluster provided an opportunity to analyze the transmission of the substituent effect through the cage and compare the results to those for analogous benzene and [*closo*-1-CB$_{11}$H$_{12}$]$^-$ derivatives. Thus, the relative NMR chemical shifts ($\Delta\delta$) for the antipodal B(10)-**H** were plotted versus the substituent σ_p values,[45] and the results are shown in Figure 11.

A Hammett plot of $\Delta\delta$ versus Hammett σ_p for ^{1}H NMR B(10)-**H** chemical shifts showed a good linear fit for several substituents (Figure 11a). The correlation factor r^2 is 0.94 for all substituents, and it increases to 0.99 if the two outlaying data points (X $=$ NH$_3$ and X $=$ Cl) are removed. This change has little effect on the slope (ρ) of the linear fit, which slightly increases from 0.70 $\pm$ 0.05 to 0.73 $\pm$ 0.02 for the smaller data set. Interestingly, the slope for the B(10)-**H** chemical shift is practically the same as that obtained for the C(4)-**H** chemical shift in monosubstituted benzene derivatives ($\rho = 0.70 \pm 0.09$) after correction for anisotropic magnetic shielding.[28,46]

The Hammett plot of B(10) and B(12)[47] ^{11}B NMR chemical shifts for {*closo*-1-CB$_9$} and {*closo*-1-CB$_{11}$},

(41) Jaffé, H. H. *Theory and Applications of Ultraviolet Spectroscopy*; Wiley: New York, 1962; pp 276−286.

(42) Kojima, M.; Nebashi, S.; Ogawa, K.; Kurita, N. *J. Phys. Org. Chem.* **2005**, *18*, 994−1000.
(43) Korolev, B. A.; Titova, S. P.; Ufimtsev, V. N. *J. Org. Chem. USSR* **1971**, *7*, 1228−1231.
(44) Uno, B.; Matsuhisa, Y.; Kano, K.; Kubota, T. *Chem. Pharm. Bull.* **1984**, *32*, 1691−1698.
(45) Hansch, C.; Leo, A.; Taft, R. W. *Chem. Rev.* **1991**, *91*, 165−195.
(46) Figeys, H. P.; Flammang, R. *Mol. Phys.* **1967**, *12*, 581−587.
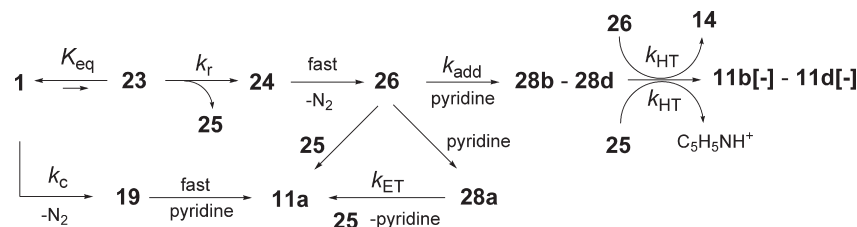(47) Jelínek, T.; Plešek, J.; Heřmánek, S.; Štíbr, B. *Collect. Czech. Chem. Commun.* **1986**, *51*, 819−829.

Figure 12. Proposed mechanism for the formation of pyridine derivatives **11**.

respectively, showed that {*closo*-1-CB$_9$} ($\rho = 12.7 \pm 1.8$) appears to be significantly more sensitive than {*closo*-1-CB$_{11}$} ($\rho = 5.3 \pm 1.3$) to the nature of the C(1) substituent (Figure 11b).

Discussion

Experiments demonstrated that the dinitrogen derivative **1** is stable in the solid state but decomposes in solutions. In MeCN, the process is slow, and the estimated half-life of **1** is $t_{1/2} = 91$ h at 25 °C and $t_{1/2} = 2$ s at 90 °C. The consistency of the measured high enthalpy of activation $\Delta H^{\ddagger}$ of 38.4 ± 0.8 kcal/mol with the calculated enthalpy change, ΔH, and the formation of a single product (**17**) support the heterolytic mechanism for the decomposition of **1** and the formation of the reactive intermediate **19** in MeCN. In addition, the unusually high experimental entropy of activation, $\Delta S^{\ddagger}$ (44.5 ± 2.5 cal/molK), is similar to the calculated ΔS value of 43.6 cal/mol K. This suggests that the dissociation process involves stretching the C_{cage}–N bond to the edge of the van der Waals contact between the atoms. Alternatively, solvent molecules are involved in the transition state, and the high value of $\Delta S^{\ddagger}$ reflects differential solvation of the ground and transition states. The proposed heterolytic unimolecular decomposition reaction of **1** is similar to that described for PhN$_2^+$ in polar aprotic solvents.[48] Interestingly, $\Delta G_{298}^{\ddagger}$ for **1** is higher by about 1.5 kcal/mol than that reported for PhN$_2^+$.[48] Also, the heterolysis of **1** has a significantly higher $\Delta S^{\ddagger}$ than that measured for PhN$_2^+$ in MeCN (18.3 cal/mol K) or in MeNO$_2$ (30.9 cal/mol K).[48]

A change of solvent significantly accelerates the transformation of **1**, which is then usually fully consumed in less than 20 h at ambient temperature. The observed increase of the reaction rate can be due to the lower activation energy for the decomposition of **1** in less polar solvents. Calculations showed that the ΔH for the formation of ylide **19** is lower by 1 kcal/mol in the pyridine dielectric medium and 3.2 kcal/mol in a vacuum relative to that in MeCN (Table 2) due to a greater dielectric stabilization of **1** than the products. Consequently, heterolysis of **1** can be nearly 20 times faster in pyridine and nearly 50 times faster in a vacuum than in MeCN, assuming the same $\Delta S^{\ddagger}$ and that the difference in ΔH of the reaction reflects the difference in $\Delta H^{\ddagger}$. Often, however, $\Delta S^{\ddagger}$ changes with the solvent (cf. $\Delta S^{\ddagger}$ for PhN$_2^+$). Thus, for heterolysis of **1** in less polar solvents, the entropy of activation may be smaller, which will partially compensate the change in $\Delta H^{\ddagger}$, and consequently less impact on the reaction rate will be observed. Alternatively, a change of mechanism can be responsible for the significantly different reaction rate.

The reaction of ylide **19** with pyridine is expected to give the N(1) adduct **11a** directly as the only or dominant product,

since the process is favored kinetically (anticipated low activation barrier) and has a large exotherm ($\Delta H = -102.6$ kcal/mol). Support for this expectation is provided by the reported smooth transformations of similar dinitrogen derivatives of the [*closo*-B$_{10}$H$_{10}$]$^{2-}$ cluster with pyridine,[2−4,6−8] and also the isolation of [*closo*-1-CB$_{11}$Me$_{11}$-1-C$_5$H$_5$N] as the only product of a reaction of the [*hypercloso*-1-CB$_{11}$Me$_{11}$] ylide with pyridine.[33] Instead, the observed distribution of products in the reaction of **1** with pyridine suggests a radical pathway, which is similar to the known Gomberg−Bachmann free-radical arylation reaction.[49] In both reactions, all *C*-substituted pyridine isomers are formed with the dominant proportions of the C(2) isomer.[34,50] The radical mechanism for the formation of **11** is supported also by computational results, which demonstrate that the formation of radical ion **26** from **1** is as feasible as the generation of Ph$^{\bullet}$ (**32**) from PhN$_2^+$, considering the difference in the treatment of ion pairs and nonionic molecules by the IPCM model.

From the mechanistic point of view, reaction of **1** in neat pyridine can proceed by either a heterolytic or homolytic pathway (Figure 12). The first and also rate-determining step in the former mechanism is a unimolecular first-order reaction, whereas the rate-limiting step in the radical pathway is pseudo-first-order formation of diazenyl radical **24**, since [pyridine] $\approx$ const $\gg$ [**1**]. At ambient temperature, the radical process appears to be significantly faster ($k_c \ll K_{eq}k_r$),[51] and the resulting radical anion **26** attacks the dominant neutral pyridine (solvent) following pseudo-first-order kinetics. This reaction is faster than the energetically more favorable (Table 4) ion recombination reaction of **26** and the pyridinium radical **25** (a second-order process), which, presumably, leads directly to the N(1) adduct **11a**. The attack of **26** on pyridine is calculated to be moderately exoergic (ΔG_{298} between −11.3 kcal/mol for **28a** and −13.7 kcal/mol for **28c**), and with a sufficiently low activation barrier, the process may be reversible, leading to the thermodynamic intermediate **28**. The subsequent electron transfer (ET) from **28a** and hydrogen transfer (HT) from **28b**−**28d** to **25**[52] and the formation of **11a** and **11b[-]**−**11d[-]**, respectively, are highly exothermic ($\Delta H > 100$ kcal/mol in the dielectric medium) and considered irreversible. Therefore, the formation of **11b** as the major component of the mixture may arise either from the kinetic preference for the formation of intermediate **28b** (if the barrier is sufficiently high and the HT

(48) Ishida, K.; Kobori, N.; Kobayashi, M.; Minato, H. *Bull. Chem. Soc. Jpn.* **1970**, *43*, 285–286.

(49) (a) Dermer, O. C.; Edmison, M. T. *Chem. Rev.* **1957**, *57*, 77–122. (b) Bachmann, W. E.; Hoffman, R. A. *Org. React.* **1944**, *2*, 224–261.

(50) Beadle, J. R.; Korzeniowski, S. H.; Rosenberg, D. E.; Garcia-Slanga, B. J.; Gokel, G. W. *J. Org. Chem.* **1984**, *49*, 1594–1603.

(51) From the steady-state approximation considering that the rate of decomposition of adduct **23** is much slower than the reverse reaction.

(52) Since [**26**] $\approx$ [**25**], radical anion **26** competes with **25** for the hydrogen from **28**, which may explain the observed low yield formation of **14**.

process is fast) or from the thermodynamic stability of **28b** (if the barrier is sufficiently low and the HT process is slow). The latter implies that the calculations underestimated the stability of **28b** by about 2 kcal/mol relative to **28c**, which is not unreasonable. In fact, all *C*-substituted intermediates have comparable calculated energies within 2 kcal/mol in the pyridine dielectric medium. It needs to be remembered that the dielectric medium significantly destabilizes **28c** and has the least effect on the energy of formation of **28b** (Table 6). Also, **28a** is the thermodynamically least favorable intermediate, which is in agreement with its practical absence among the reaction products. A similar discrepancy between the calculated thermodynamic stability of the radical intermediates **33** and the distribution of the products **30** is found for the phenylation of pyridine (Table 6). Again, this may indicate that product formation is governed by kinetics (irreversible processes), or the relative energies are calculated with an error of ±2 kcal/mol.

At higher temperatures, the rate of formation of the ylide **19** becomes competitive with that of generation of the radical anion **26** ($k_c \sim K_{eq}k_r$), and consequently, the N(1) isomer **11a** is formed in substantial amounts along with its *C*-isomers (Table 1).

In dilute solutions of pyridine in benzene, both mechanisms, the heterolytic and the homolytic decomposition of **1**, may operate at the same time, as is indicated by the formation of N(1) and C(2) isomers (**11a** and **11b**, respectively) in comparable amounts (Table 1). The lower dielectric permittivity of benzene may increase the rate of the formation of **19**, while the lower concentration of pyridine in solution could decrease the rate of formation of radical anion **26**. Consequently, both intermediates, **19** and **26**, can be formed at similar rates. The radical anion is expected to react easily with both pyridine and benzene, leading to **11b** and [*closo*-1-CB$_9$H$_9$-1-Ph]$^-$ (**16**), respectively. Calculations support this expectation and demonstrate that both addition reactions of **26** to benzene and pyridine at the C(2) position have comparable exotherms ΔH of -24.9 and -23.4 kcal/mol, respectively, in the pyridine dielectric medium. The ylide **19** is expected to attack pyridine's N atom, leading to **11a** and benzene to form **16**. The formation of the latter presumably follows the mechanism proposed for the electrophilic substitution of aromatic hydrocarbons with the [*hypercloso*-1-CB$_{11}$Me$_{11}$] ylide[33] and involves an three-center, two-electron bond intermediate analogous to **22** (Figure 4).

In methylene chloride solutions, the situation is similar, and transformation of **1** may follow both mechanistic pathways involving both reactive intermediates. The radical anion **26** is expected to react with pyridine, giving **11b**, and to abstract hydrogen from the solvent, giving the observed parent cluster **14**. It may also transfer a Cl atom to form the chloride [*closo*-1-CB$_9$H$_9$-1-Cl]$^-$ (**15**). Calculations indicate that abstractions of a chlorine atom and a hydrogen from CH$_2$Cl$_2$ are both exothermic processes ($\Delta G_{298} = -19.3$ and -18.6 kcal/mol, respectively) in a dielectric medium ($\varepsilon = 13.3$) and more favorable energetically than addition to the C(2) of pyridine ($\Delta G_{298} = -12.3$ kcal/mol). The ylide **19** formed in an unassisted thermolysis of **1** gives the N(1) adduct **11a** and may also abstract Cl$^-$ from the solvent, forming the chloride [*closo*-1-CB$_9$H$_9$-1-Cl]$^-$ (**15**). A subsequent reaction of the resulting +CH$_2$Cl with pyridinium leads to *N*-(chloromethyl)pyridinium, which was observed

as the counterion in the crystal structure of the isolated chloride **15**.[53]

Results of reactions of **1** in dilute solutions of pyridine in MeCN are also consistent with the dual mechanism and involvement of the two reactive intermediates. In addition to **17** and **11a**, products expected for trapping of the ylide **19**, the reaction mixture contained several unidentified signals, which are presumably related to reactions of radical ion **26** with the solvent and pyridine. Interestingly, the rate of decomposition of **1** in the MeCN/pyridine solution is approximately the same as the rate in pure MeCN.

The mechanism of pyridine-induced radical reactions of **1** is similar to the accepted mechanism of free-radical arylation of pyridine with benzenediazonium salts.[34−36,54] In both cases, a stable adduct of pyridine to the N$_2$ group was located on the PES (compounds **23** and **29**). The relatively high energy of adducts **23** and **29** suggests that they are transient species formed at low concentrations, which give rise to the radical ion pairs. Further studies of reactions of arenediazonium salts indicated that the radical/cationic pathway correlates with the nucleophilicity of the solvent[36,54] and does not necessarily involve a stable transient adduct but rather involves an intermolecular electron transfer (outer-sphere ET).[36] Thus, pyridine has one of the highest nucleophilicity parameters, whereas acetonitrile has one of the lowest nucleophilicity parameters.[54,55] Therefore, the former may induce radical generation, while the latter will favor cationic processes. This is indeed observed experimentally for the decomposition of both **1** (present work) and benzenediazonium salts[56−60] for which the corresponding acetamides are the main products in MeCN solutions (see Scheme 7).

The propensity of a nucleophile to induce radical reactions of **1** and PhN$_2^+$ can be assessed from the energetics of ET between the diazonium and the donor calculated from ionization potential (I_p) and electron affinity (E_a) for a gas-phase reaction, or from oxidation (E^{ox}) and reduction (E^{red}) potentials in solutions (Table 8). Calculations demonstrate that, while the E_a for the two electrophiles, **1** and PhN$_2^+$, are different in the gas phase by over 3.5 eV, they are practically the same in MeCN solutions. The dielectric medium stabilizes charged molecules, and consequently, the addition of an electron to **1** becomes more favorable, while the reduction of PhN$_2^+$ is less exothermic in MeCN.

The calculated I_p values for the five reagents compare well with the experimental data[61] with a systematic underestimation by about 0.3 eV. In the MeCN dielectric medium, the calculated I_p values are lowered by 2−3 eV relative to the gas phase. A comparison of the calculated ionization values to the experimental electrochemical data (Table 8) can be made only at a qualitative level, since all investigated processes

(53) Carr, M. J.; Kaszynski, P.; Franken, A.; Kennedy, J. D. Manuscript in preparation.

(54) Szele, I.; Zollinger, H. *Helv. Chim. Acta* **1978**, *61*, 1721–1729.

(55) Maria, P.-C.; Gal, J.-F. *J. Phys. Chem.* **1985**, *89*, 1296–1304.

(56) Kice, J. L.; Gabrielsen, R. S. *J. Org. Chem.* **1970**, *35*, 1004–1015.

(57) Makarova, L. G.; Nesmeyanov, A. N. *Bull Akad. Sci. USSR, Div. Chem. Sci.* **1954**, 887–891.

(58) Kobayashi, M.; Minato, H.; Yamada, E.; Kobori, N. *Bull. Chem. Soc. Jpn.* **1970**, *43*, 215–219.

(59) Kobayashi, M.; Minato, H.; Kobori, N. *Bull. Chem. Soc. Jpn.* **1970**, *43*, 219–223.

(60) Kobori, N.; Kobayashi, M.; Minato, H. *Bull. Chem. Soc. Jpn.* **1970**, *43*, 223–225.

(61) NIST Standard Reference Database Number 69 (http://webbook.nist.gov/chemistry/) and references therein.

Table 8. Calculated Adiabatic Electron Affinity (E_a) and Ionization Potential (I_p) and Experimental Electrochemical Reduction/Oxidation Potentials for Selected Compounds

compound	calculated[a]			experimental[b]	
	$\varepsilon = 1^c$	$\varepsilon = 13.3^d$	$\varepsilon = 36.6^d$	E_{pa}^{ox}/V	E_{pc}^{red}/V
		electron affinity/eV			
1	2.11	3.69	3.76		−0.54
$C_6H_5N_2^+$	5.84	3.86	3.76		−0.16[e]
		ionization potential/eV			
Me_2S	8.29 (8.69)[f]	5.91	5.77	1.78[g]	
Me_2NCHS	7.94 (8.2)[f]	5.93	5.83	1.25	
pyridine	8.95 (9.26)[f]	6.82	6.72	lit. ~1.5[h]	
CH_2Cl_2	10.93 (11.33)[f]	8.40	8.27	~1.8[i]	
MeCN	12.10 (12.20)[f]	9.28	9.42	~2.4[i]	

[a] MP2/6-31G(d,p)//B3LYP/6-31G(d,p) level with DFT enthalpic corrections. [b] Peak potential recorded in MeCN (0.05 M Bu$_4$NPF$_6$) vs SCE. [c] Vacuum calculations. [d] IPCM solvation model. [e] Lit. −0.17 (MeCN, SCE) ref 63. [f] Experimental data taken from ref 61. [g] Lit.[62] +1.71 V vs SCE. [h] Recorded in neat pyridine 64. [i] Solvent electrochemical limit; ref 65.

are irreversible in solution and the observed current peak potentials do not represent thermodynamic processes. The calculated ionization potentials I_p generally follow the trend in experimental anodic peak potentials E_{pa}^{ox} for all reagents, with the exception of Me_2S (Table 8). In agreement with calculations, the lowest oxidation potential is observed for the thioformamide and the highest for MeCN. The experimental E_{pa}^{ox} for Me_2S is higher by over 0.5 V than predicted, presumably due to complex chemical behavior of the radical cation.[62]

A comparison of calculated electron affinities with the electrochemical data shows that the reduction of **1** is more cathodic by 0.39 V than that of PhN_2^+. The discrepancy between calculated solution E_a values and observed E_{pc} values (Table 8) is presumably due to the difference in ion solvation (cation vs anion) and solvent reorganization energy.

Calculated data in Table 9 demonstrate that ET between pyridine and PhN_2^+ (outer-sphere process) and the formation of a radical ion pair are endothermic in pyridine (ΔG_{298} = 66.3 kcal/mol) and practically the same in MeCN solution (Table 9), which corresponds to the difference in the measured current peak potentials of $\Delta E_p \approx 1.7$ V (Table 8). The same analysis for **1** and pyridine gives a similar value for the ET process in MeCN (ΔG_{298} = 65.3 kcal/mol) but a larger experimental electrochemical potential ($\Delta E_p \approx$ 2.0 V).

Calculations suggest that the ET process between **1** and Me_2S and also Me_2NCHS is more favorable, and it should be faster than that with pyridine (Table 9). Both sulfur reagents have markedly lower I_p values relative to pyridine, and consequently ΔG_{298} values for electron transfer to **1** are lower

(62) Cottrell, P. T.; Mann, C. K. *J. Electrochem. Soc.* **1969**, *116*, 1499–1503.

(63) Andrieux, C. P.; Pinson, J. *J. Am. Chem. Soc.* **2003**, *125*, 14801–14806.

(64) Turner, W. R.; Elving, P. J. *Anal. Chem.* **1965**, *37*, 467–469.

(65) Baizer, M. M.; Lund, H. *Organic Electrochemistry*, 2nd ed.; Marcel Dekker: New York, 1983 and references therein.
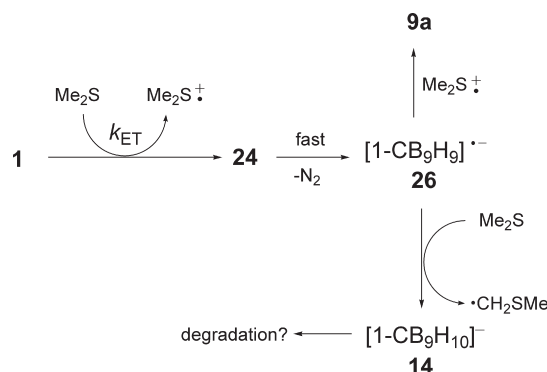
Table 9. Calculated Free Energy Change ΔG_{298} for the Electron Transfer Process between **1** and Selected Solvents[a]

$$R\text{-}N_2^+ + :Nu \rightarrow R\text{-}N_2^\bullet + \overset{\bullet}{}^+Nu$$

R	[*closo*-1-CB$_9$H$_9$]$^-$ (**1**)			Ph−		
Nu	$\varepsilon = 1^b$	$\varepsilon = 13.3^c$	$\varepsilon = 36.6^c$	$\varepsilon = 1^b$	$\varepsilon = 13.3^c$	$\varepsilon = 36.6^c$
Me_2S	138.8	47.4	43.0	53.7	44.4	43.9
Me_2NCHS	132.3	49.6	45.8	47.2	46.6	46.7
pyridine	154.7	69.2	65.3	69.6	66.3	66.2
CH_2Cl_2	200.9	106.0	101.4	115.8	103.0	102.3
MeCN	227.3	125.7	127.5	142.2	122.8	128.4

[a] MP2/6-31G(d,p)//B3LYP/6-31G(d,p) level with DFT thermodynamic corrections. Energies in kcal/mol. [b] Vacuum calculations. [c] IPCM solvation model.

by 20 kcal/mol, or 1/3, than those for pyridine (Table 9). This is consistent with a smaller ΔE_p of 1.79 V (Table 8) for the reaction of **1** and Me_2NCHS and indicates that the formation of **10** and possibly also **9a** may involve a radical process, which begins with outer-sphere ET (intermolecular) and formation of the radical ion pair.[66] According to the proposed radical mechanism of reaction of **1** with Me_2S, the radical ion pair collapses to form the product **9a** (Figure 13). Since the concentration of the ions is small and the rate of this bimolecular process is low, other processes take place, such as a loss of proton and presumably an abstraction of H. Consequently, the adduct **9a** is isolated only in 40% yield, with the rest of the precursor forming polymeric/decomposition products. It is expected that the reaction of **19** with Me_2S would give the adduct **9a** in a much higher yield.

The reaction with Me_2NCHS is much more efficient. The thionocarbonyls are known to react smoothly with *C*-centered radicals, often in a chain process, in which the weak S=C bond is eliminated.[67] Thus, it can be postulated that radical ion **26** preferentially attacks the sulfur atom, giving rise to the *C*-centered transient radical **35** stabilized by both the N and S atoms (Figure 14). Subsequent ET to the Me_2NCHS radical cation gives product **10**. Overall, the preparation of dialkylsufonium derivatives such as **9** is most efficiently done in a two-step process using **10** as the intermediate.

The intermediacy of ylide **19** in the formation of **9a** or **10** cannot be excluded, and clearly more detailed studies are necessary for a better understanding of the mechanism and intermediates involved in transformations of **1**.

Solvents with high a I_p (>10 eV) and E_{pa}, such as MeCN and CH_2Cl_2, are not expected to transfer an electron to **1** and induce its radical transformations. Therefore, decomposition of **1** in these solvents is likely to involve ylide **19**, as postulated for thermolysis in MeCN. The products of reactions of **1** in CH_2Cl_2 and also benzene are largely intractable, which may be a result of their extensive decomposition caused by an unsolvated counterion, either $+CH_2Cl$ (in reaction with CH_2Cl_2) or H^+ (in reaction with benzene). The yields of **15** and **16** may be improved by using a non-nucleophilic base with a high I_p in the reaction medium.

Overall, slow decomposition of **1** through ylide **19** can be expected in solvents such as $MeNO_2$ with a high I_p, for which

(66) No stable adduct of Me_2S to **1** nor to PhN_2^+ was located on the PES with the DFT method.

(67) Barton, D. H. R.; Crich, D.; Motherwell, W. B. *Tetrahedron* **1985**, *41*, 3901–3924.

Figure 13. Proposed mechanism for the formation of **9a**.

Figure 14. Proposed mechanism for the formation of **10**.

adducts to **19** are relatively stable zwitterions (do not produce aggressive electrophiles), and have been demonstrated to promote the heterolytic unimolecular decomposition of PhN_2^+.[48] On the other hand, reagents with a high nucleophilicity and low I_p, such as amines and sulfur compounds, are likely to induce radical transformations of **1**.

Analysis of electronic absorption spectra and chemical shifts revealed significant similarities between the [*closo*-1-CB_9H_{10}]⁻ and benzene. Thus, electronic absorption spectra demonstrated substantial electronic communication between the {*closo*-1-CB_9} cage and π substituents. This is consistent with our previous experimental and theoretical studies for the derivatives of $[B_{10}H_{10}]^{2-}$ and $C_2B_8H_{10}$.[6−8,11,68−70] In the absence of π susbtituents, the compounds are practically UV-transparent. Since the cage is negatively charged, the electronic excitations of zwitterionic derivatives such as **1** and **11a** involve the cage-to-substituent transitions, which exhibit strong solvatochromism[6,8] and may find applications as NLO chromophores.

The Hammett analysis of NMR chemical shifts demonstrated a similar ability to transmit electronic effects through the [*closo*-1-CB_9H_{10}]⁻ cage and benzene ring, which is significantly higher than that found for the [*closo*-1-$CB_{11}H_{12}$]⁻ derivatives. The stronger antipodal effect[71,72] observed in the {*closo*-1-CB_9} cluster relative to the {*closo*-1-CB_{11}} may be related to the smaller size and higher electron density for the former as compared to the latter. The only other Hammett correlation previously reported for boron clusters was for ^{13}C NMR chemical shifts of *C*-arylated *p*-carborane derivatives.[73] A comparison[28] of the slope (ρ values) reported[73] for 1-aryl-*p*-carboranes with that for ^{13}C NMR chemical shifts of 4-substituted biphenyls demonstrates that the transmission of a substituent effect through the 12-vertex carborane cage is about 70% as effective as through the benzene ring.[28] This finding is consistent with results presented in Figure 11.
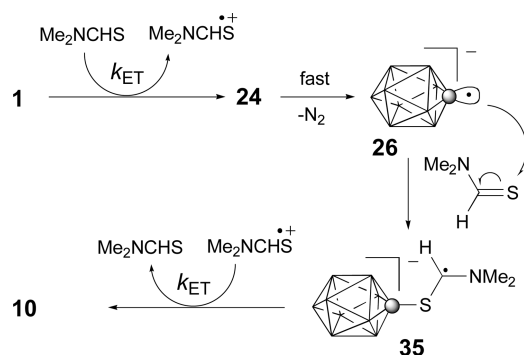
Summary and Conclusions

The present studies describe an alternative and reliable method for the preparation of amine **2** and dinitrogen derivative **1** and provide good understanding of the properties of the latter and its usefulness as a synthetic intermediate in the preparation of more complex derivatives, including liquid crystals. The method for the formation of amino functionality through the COOH group permits the introduction of an antipodal substituent at the stage of [*closo*-2-CB_9H_9-2-COOH]⁻.[16] Such compounds are being currently investigated in our laboratory.

In many respects, dinitrogen derivative **1** displays behavior similar to that of benzenediazonium salt; it has similar stability, undergoes diazo coupling, reacts with sulfur nucleophiles, with pyridine gives *C*-substituted products, and undergoes heterolysis in MeCN, forming *N*-substituted acetamide. A detailed analysis of the experimental data and computational results revealed two possible mechanisms for the transformations of **1**: the closed-shell zwitterionic pathway through ylide **19** and an open-shell radical pathway involving radical anion **26**. The latter is analogous to the nucleophile-induced decomposition of PhN_2^+ and operates for reagents and solvents, which are good nucleophiles and electron donors (low I_p and low $E_{1/2}^{ox}$). In the absence of electron donors (reagents with high I_p and $E_{1/2}^{ox}$), dinitrogen **1** undergoes heterolytic cleavage of N_2, and the resulting ylide **19** gives products of electrophilic addition. The properties and reactivity, such as the preferential formation of the *N*-adduct with pyridine, of **19** are very similar to those observed before for the [*hypercloso*-1-$CB_{11}Me_{11}$] ylide. Clearly, more kinetic experiments need to be done for a better understanding of the reactivity of **1** and to provide more evidence for the involvement of ylide **19** and radical anion **26** in transformations of **1**.

Experimental results demonstrated that **1** serves as a convenient precursor for the preparation of dialkylsulfonium derivatives such as **9b**; the two-step process through **10**, a masked thiol generated in situ, is more efficient due to a higher yield of the first step. Also, the diazocoupling of **1**, leading to azophenols such as **8**, is an efficient process, which has already been exploited for the preparation of ionic liquid crystals.[15] In contrast, the preparation of *N*-substituted pyridine **11a**, which is of interest for the investigation of molecular materials, is a low-yield process of little synthetic value at present.

Spectroscopic investigation indicates significant electronic interactions between the {*closo*-1-CB_9} cage and π substituents, which indicates a possibility of control of photophysical properties in specifically designed molecular materials.

(68) Kaszynski, P. In *Anisotropic Organic Materials—Approaches to Polar Order*; Glaser, R., Kaszynski, P., Eds.; ACS Symposium Series: Washington, DC, 2001; Vol. *798*, pp 68−82.

(69) Pakhomov, S.; Kaszynski, P.; Young, V. G., Jr. *Inorg. Chem.* **2000**, *39*, 2243−2245.

(70) Kaszynski, P.; Kulikiewicz, K. K.; Januszko, A.; Douglass, A. G.; Tilford, R. W.; Pakhomov, S.; Patel, M. K.; Radziszewski, G. J.; Young, V. G., Jr. Manuscript in preparation.

(71) (a) Hermanek, S.; Plesek, J.; Gregor, V.; Stirb, B. *Chem. Commun.* **1977**, 561−563. (b) Hermanek, S. *Chem. Rev.* **1992**, *92*, 325−362.

(72) Bühl, M.; Schleyer, P. v. R.; Havlas, Z.; Hnyk, D.; Hermanek, S. *Inorg. Chem.* **1991**, *30*, 3107−3111.

(73) Fox, M. A.; MacBride, H. J. A.; Peace, R. J.; Wade, K. *J. Chem. Soc., Dalton Trans.* **1998**, 401−411.

Overall, results demonstrate that dinitrogen **1** is an attractive compound for further mechanistic investigation and synthetic applications.

Computational Details

Quantum-mechanical calculations were carried out with the B3LYP[74,75] and MP2(fc)[76] methods with the 6-31G(d,p) basis set using the Gaussian 98 computational package.[77] Geometry optimizations were undertaken using appropriate symmetry constraints and tight convergence limits. Vibrational frequencies were obtained with the B3LYP/6-31G(d,p) method and were used to characterize the nature of the stationary points and to obtain thermodynamic parameters. Zero-point energy corrections were scaled by 0.9806.[78] A population analysis for single-point calculations (MP2// DFT) was performed using the Density keyword. For MP2-level calculations of open-shell species, the spin-projected energies were used for comparative studies. The IPCM solvation model[79] was used with default parameters.

Experimental Details

Reagents and solvents were obtained commercially. Solvents were dried and deoxygenated before use, and reagents were used as supplied. $ZnCl_2$ was dried by heating at ∼100 °C under a vacuum. Reactions were carried out under dry Ar and subsequent manipulations conducted in the air. NMR spectra were obtained at 128.4 MHz ([11]B), 100.6 MHz (^{13}C), and 400.1 MHz (^{1}H) in CD_3CN unless otherwise specified. ^{1}H NMR and ^{13}C NMR spectra were referenced to the solvent. ^{11}B NMR chemical shifts are relative to the resonance of an external boric acid sample in CH_3OH that was set to 18.1 ppm. IR spectra were recorded in the solid state using an AT-IR accessory.

UV spectra were recorded in UV-grade CH_3CN. All compounds were at a concentration of $0.7–5 \times 10^{-5}$ M. Extinction coefficients were obtained by fitting the maximum absorbance against concentration in agreement with Beer's law.

Electrochemical analysis was conducted in dry MeCN with Bu_4NPF_6 (0.05 M) as the supporting electrolyte and using a freshly polished glassy carbon working electrode with the Ag/AgCl reference electrode. The scanning rate was 1 V/s. Following literature recommendations,[63] the concentrations of compounds **1** and PhN_2^+ were set at 0.6 mM, and the reported data were taken from the first scan. Continuous scanning of the electrochemical window (+0.7 to −1.0 V) resulted in shifting of the observed cathodic peak to more negative potentials due to electrode passivation by the electrografting of Ph• or [*closo*-1-CB_9H_9] radicals.

Peak potentials were referenced by adding small amounts of ferrocene to the solution, and the E-chem scan for each compound was referenced to the ferrocene couple, which was assumed to be 0.31 V versus SCE (MeCN, 0.2 M $LiClO_4$).[80]

Preparation of [*closo*-1-CB₉H₉-1-N₂] (1). A suspension of [*closo*-1-CB_9H_9-1-NHBoc]⁻NEt₄⁺ (**4a[NEt₄]**, 0.21 g, 0.57 mmol) in a 1:3 mixture of concentrated HCl in CH_3OH (10 mL) was gently heated until all of the solid was dissolved, and stirring was continued at room temperature for 18 h. Water (15 mL) was added, and CH_3OH was removed in vacuo. Concentrated HCl (3 mL) was added, and [*closo*-1-CB_9H_9-1-NH₃] (**2**) was extracted into Et_2O (3 × 15 mL). The organic layers were combined, dried (Na_2SO_4), and evaporated in vacuo to give 0.120 g (166% yield) of crude amine **2** as a transparent glassy solid. ^{1}H NMR: δ 0.61 (q, J = 145 Hz, 4H), 1.74 (q, J = 156 Hz, 4H), 5.46 (q, J = 156 Hz, 1H), 8.55 (s) [lit data:[12] ^{1}H NMR: δ 0.81 (4H), 2.34 (4H), 5.53 (1H), 10.15 (3H)]. ^{13}C NMR: δ 66.6. ^{11}B NMR: δ −25.5 (d, J = 141 Hz, 4B), −16.8 (d, J = 152 Hz, 4B), 29.1 (d, J = 159 Hz, 1B) [lit data:[12] ^{11}B NMR: δ −25.8 (4B), −16.8 (4B), 29.2 (1B)]. IR: 3182 and 3162 (N−H) cm⁻¹.

Crude amine **2** was dissolved in a 1:1 mixture of $AcOH/H_2O$ (1 mL), and an aqueous solution of $NaNO_2$ (0.043 g, 0.63 mmol) in H_2O (2 mL) was added dropwise (∼1 drop/sec) at 0 °C. The reaction temperature was maintained for 30 min. H_2O (2 mL) was added, and a precipitate was filtered and dried, giving 0.066 g (80% yield) of [*closo*-1-CB_9H_9-1-N₂] (**1**) as a white crystalline solid: dec ∼87 °C (ΔH = 148 kJ/mol, DSC). ^{1}H NMR (CD_3CN): δ 0.96 (q, J = 150 Hz, 4H), 2.51 (q, J = 167 Hz, 4H), 6.65 (q, J = 164 Hz, 1H). ^{1}H NMR (benzene-d_6): δ 1.10−3.20 (m, 8H), 7.87 (q, J = 170 Hz, 1H). ^{11}B NMR (CD_3CN): δ −22.1 (d, J = 149 Hz, 4B), −8.6 (d, J = 167 Hz, 4B), 51.3 (d, J = 167 Hz, 1B). ^{11}B NMR (benzene-d_6): δ −20.6 (d, J = 147 Hz, 4B); −6.8 (d, J = 163 Hz, 4B), 57.0 (d, J = 179 Hz, 1B). IR: 2250 (N₂) cm⁻¹. UV (CH_3CN): λ_{max} 250 nm (log ε = 3.82).

Preparation of [*closo*-1-CB₉H₉-1-NHBoc]⁻ NEt₄⁺ (4a). A suspension of [*closo*-1-CB_9H_9-1-COOH]⁻NEt₄⁺ (**3[NEt₄]**, 1.14 g, 3.88 mmol) [^{11}B{^{1}H} NMR: δ −23.6 (4B), −15.4 (4B), 34.2 (1B); IR 1678 (C=O) cm⁻¹] in anhydrous CH_2Cl_2 (10 mL) was treated with 2 M $(COCl)_2$ in CH_2Cl_2 (2.2 mL, 4.3 mmol). Vigorous bubbling of CO and CO_2 gases was observed, followed by the dissolution of the substrate and the formation of a slight yellow solution. The solution was stirred for 75 min at room temperature, filtered to remove insoluble particulates, and the solvent removed in vacuo to give 1.20 g of crude [*closo*-1-CB_9H_9-1-COCl]⁻NEt₄⁺ (**5[NEt₄]**) as a white solid. ^{11}B {^{1}H} NMR: δ −23.1 (4B), −13.5 (4B), 38.5 (1B). IR: 1776 (C=O) cm⁻¹.

Crude [*closo*-1-CB_9H_9-1-COCl]⁻NEt₄⁺ (**5[NEt₄]**, 1.20 g, 3.85 mmol) was dissolved in anhydrous CH_2Cl_2 (10 mL) and added via syringe to solid anhydrous $ZnCl_2$ (0.052 g, 0.38 mmol) under a N₂ atmosphere. The reaction mixture was cooled to 0 °C, and Me_3SiN_3 (0.55 mL, 4.2 mmol) was added. The reaction mixture was stirred at 0 °C for an additional 30 min, after which it was warmed to room temperature and stirred for 4 h. The reaction mixture was poured into ice-cold H_2O (50 mL) and extracted with CH_2Cl_2 (3 × 30 mL). The organic layers were combined, dried ($MgSO_4$), and filtered, and the solvent was removed in vacuo, giving 1.11 g of [*closo*-1-CB_9H_9-1-CON₃]⁻NEt₄⁺ (**6[NEt₄]**) as a white crystalline solid. ^{11}B{^{1}H} NMR: δ −23.3 (4B), −14.8 (4B), 36.4 (1B). IR: 2360, 2339 and 2142 (N₃), 1691 (C=O) cm⁻¹. The crude product was contaminated with about 15% carboxylic acid **3[NEt₄]**.

Crude [*closo*-1-CB_9H_9-1-CON₃]⁻NEt₄⁺ (**6[NEt₄]**, 1.11 g, 3.49 mmol) was dissolved in anhydrous CH_3CN (15 mL) and refluxed for 1 h. The reaction was cooled to room tmeperature, the solvent removed, and the residue dried in vacuo, giving 1.11 g of crude [*closo*-1-CB_9H_9-1-NCO]⁻NEt₄⁺ (**7[NEt₄]**) as a slight

(74) Becke, A. D. *J. Chem. Phys.* **1993**, *98*, 5648–5652.
(75) Lee, C.; Yang, W.; Parr, R. G. *Phys. Rev. B* **1988**, *37*, 785–789.
(76) (a) Møller, C.; Plesset, M. S. *Phys. Rev.* **1934**, *46*, 618–622. (b) Head-Gordon, M.; Pople, J. A.; Frisch, M. J. *Chem. Phys. Lett.* **1988**, *153*, 503–506.
(77) Frisch, M. J.; Trucks, G. W.; Schlegel, H. B.; Scuseria, G. E.; Robb, M. A.; Cheeseman, J. R.; Zakrzewski, V. G.; Montgomery, J. A., Jr.; Stratmann, R. E.; Burant, J. C.; Dapprich, S.; Millam, J. M.; Daniels, A. D.; Kudin, K. N.; Strain, M. C.; Farkas, O.; Tomasi, J.; Barone, V.; Cossi, M.; Cammi, R.; Mennucci, B.; Pomelli, C.; Adamo, C.; Clifford, S.; Ochterski, J.; Petersson, G. A.; Ayala, P. Y.; Cui, Q.; Morokuma, K.; Malick, D. K.; Rabuck, A. D.; Raghavachari, K.; Foresman, J. B.; Cioslowski, J.; Ortiz, J. V.; Baboul, A. G.; Stefanov, B. B.; Liu, G.; Liashenko, A.; Piskorz, P.; Komaromi, I.; Gomperts, R.; Martin, R. L.; Fox, D. J.; Keith, T.; Al-Laham, M. A.; Peng, C. Y.; Nanayakkara, A.; Challacombe, M.; Gill, P. M. W.; Johnson, B.; Chen, W.; Wong, M. W.; Andres, J. L.; Gonzalez, C.; Head-Gordon, M.; Replogle, E. S.; Pople, J. A. *Gaussian 98*, revision A.9; Gaussian, Inc.: Pittsburgh, PA, 1998.
(78) Scott, A. P.; Radom, L. *J. Phys. Chem.* **1996**, *100*, 16502–16513.
(79) Foresman, J. B.; Keith, T. A.; Wiberg, K. B.; Snoonian, J.; Frisch, M. J. *J. Phys. Chem.* **1996**, *100*, 16098–16104.

(80) Bard, A. J.; Faulkner, L. R. *Electrochemical Methods: Fundamentals and Applications*, 2nd ed.; Wiley: Hoboken, NJ, 2001.

yellow solid. $^{11}B\{^1H\}$ NMR: δ −26.1 (4B), −16.0 (4B), 25.1 (1B). IR: 2262 (N=C=O).

A solution of anhydrous *tert*-butanol (15 mL), anhydrous CH_3CN (5 mL), and crude [*closo*-1-CB$_9$H$_9$-1-NCO]$^-$NEt$_4^+$ (**7[NEt$_4$]**, 1.04 g, 3.58 mmol) was stirred at 90 °C for 2 h, after which solvents were removed, leaving 1.20 g of crude [*closo*-1-CB$_9$H$_9$-1-NHBoc]$^-$NEt$_4^+$ (**4a[NEt$_4$]**) as a yellow solid. The crude solid was dissolved in CH_2Cl_2 and passed through a silica gel plug buffered with 1% NEt$_3$ in CH_2Cl_2. Elution with a buffered CH_3CN/CH_2Cl_2 solution (1% NEt$_3$, 20% CH_3CN, 79% CH_2Cl_2) afforded 0.68 g (48% yield based on starting acid **3[NEt$_4$]**) of pure [*closo*-1-CB$_9$H$_9$-1-NHBoc]$^-$NEt$_4^+$ (**4a[NEt$_4$]**) as a light yellow solid: mp 140 °C. ^1H NMR: δ 0.45 (q, $J = 143$ Hz, 4H), 1.19 (t, $J = 7.3$ Hz, 12H), 1.49 (s, 9H), 1.67 (q, $J = 156$ Hz, 4H), 3.14 (q, $J = 7.3$ Hz, 8H), 5.07 (q, $J = 151$ Hz, 1H), 7.12 (s, 1H). ^{13}C NMR: δ 7.7 (N$^+$CH$_2$**C**H$_3$), 28.6 (C(**C**H$_3$)$_3$), 47.3 (**C**(CH$_3$)$_3$), 53.0 (N$^+$**C**H$_2$CH$_3$), 156.0 (C=O). Carbon associated with the {*closo*-1-CB$_9$} cluster was not observed. Minor signals at 9.0 and 53.5 ppm were attributed to excess NEt$_4^+$Br$^-$. ^{11}B NMR: δ −26.2 (d, $J = 135$ Hz, 4B), −17.2 (d, $J = 152$ Hz, 4B), 23.8 (d, $J = 158$ Hz, 1B). IR: 3505 (N−H), 1737

(C=O) cm^{-1}. Anal. Calcd for $C_{14}H_{39}B_9N_2O_2$: C, 46.10; H, 10.78; N, 7.38. Found: C, 46.26; H, 10.76; N, 7.53.

Subsequent fractions produced 0.56 g of a 30:70 mixture of [*closo*-1-CB$_9$H$_9$-1-COOH]$^-$NEt$_4^+$ (**3[NEt$_4$]**) and [*closo*-1-CB$_9$H$_9$-1-NH$_2$]$^-$NEt$_4^+$ (**2[NEt$_4$]**). ^1H NMR: δ 1.23 (t, $J = 7.2$ Hz, 12H), 3.19 (q, $J = 8.0$ Hz, 8H), 7.31 (s, 2H). ^{11}B $\{^1H\}$ NMR: δ −26.1 (4B), −17.1 (4B), 24.1 (1B), [lit.[12] data for (**2[NHEt$_3$]**): ^1H NMR: δ 0.91 (4H), 1.69 (4H), 5.40 (1H), 8.52 (2H). ^{11}B NMR: δ −25.8 (4B), −17.2 (4B), 26.0 (1B)].

Supporting Information Available: Experimental procedures for the reactions of **1** and analytical data for products, COSY spectra for **11c[H]** and **11d[H]**, kinetic data for the decomposition of **1**, Hammett correlation data, and details of computational results. This material is available free of charge via the Internet at http://pubs.acs.org.